Fetal Programming from Sub-Lethal Radiation: Glucose Metabolism in the Liver and Brown Adipose Tissue

A thesis presented to
The Faculty of Graduate Studies
of
Lakehead University
by
CAITLUND DAVIDSON

In partial fulfillment of requirements
for the degree of
Master of Science in Biology

May 30th, 2018

Abstract

Exposure to ionizing radiation contributing to negative health outcomes is a widespread concern among the public, scientific community, and workers in the nuclear energy industry and diagnostic imaging field. However, the impact of sub-lethal exposures remains contentious particularly in pregnant women who represent a vulnerable group. The fetal programming hypothesis states that an adverse in-utero environment or stress during development of an embryo or fetus can result in permanent physiologic changes often resulting in progressive metabolic dysfunction with age. Various models of fetal programming present similar outcomes with offspring demonstrating alterations in birth weight. Low birth weight predisposes offspring to insulin resistance and impaired glucose metabolism. To assess the effects of sub-lethal dose radiation on fetal programming of glucose metabolism, pregnant C57Bl/6J mice were irradiated at 1000 mGy and compared to a sham irradiated group. Female offspring born to dams irradiated at 1000 mGy had: 1) increased liver weights, 2) increased hepatic protein expression of suppressor of cytokine signaling 3 (SOCS3) and phosphoenolpyruvate carboxykinase (PEPCK), and 3) increased ^{18}F-fluorodeoxyglucose (^{18}F-FDG) uptake in interscapular brown adipose tissue (IBAT) measured by positron emission tomography (PET). Male offspring born to irradiated dams showed non-significant reductions in SOCS3 and PEPCK protein expression in the liver and increased hepatic triglycerides. Radiation exposure to 1000 mGy caused no change in plasma triglycerides, however significant sex differences were observed. Female IBAT phosphorylated protein kinase B (Akt) to total Akt ratio and phosphorylated glycogen synthase kinase 3 beta (GSK3β) to total GSK3β ratio did not increase significantly with treatment suggesting insulin signaling is not responsible for the increase in tissue specific ^{18}F-fluorodeoxyglucose (^{18}F-FDG) uptake. It is likely that the β-adrenergic pathway is responsible for the increased IBAT glucose uptake observed in the female offspring from the increase in phosphorylated GSK3β and uncoupling protein 1 (UCP1) protein expression. While non-significant, these measures account for only a single time point in the rodent lifespan. The results of this study indicate

alterations in glucose uptake and metabolism are significant in mice at 4 months of age. These findings suggest that sub-lethal dose radiation alters glucose metabolism in the IBAT and liver of offspring and changes may progress with age.

Lay Summary

Faculty and students in the Department of Biology at Lakehead University are bound together by a common interest in explaining the diversity of life, the fit between form and function, and the distribution and abundance of organisms. This research supplements the lack of data available for the physiological effects of a sub-lethal dose of radiation exposure during pregnancy on the fetus when it reaches adult life. Changes caused by radiation may not be present at birth or visible making it difficult to detect alterations. With age, the development and progression of metabolic disease is a potential outcome. Little is known about metabolic changes that occur due to sub-lethal radiation exposure and if they present a risk or can be beneficial. While C57Bl/6J mice are considered radioresistant, a sub-lethal dose of radiation to these mice is assumed to be equivalent to a low dose exposure in humans. The findings of this study suggest that insulin resistance may result from sub-lethal radiation exposure in mice. Increased glucose uptake in interscapular brown adipose tissue (IBAT) is usually beneficial as it indicates increased energy expenditure, correlates inversely with body mass index and is a target for lowering the prevalence of obesity. In this study, it may be an indicator of compensation for alterations in glucose metabolism. Sexual dimorphism was apparent suggesting that female offspring are more susceptible to alterations in glucose metabolism that will likely become more pronounced with age. The results from this study may provide knowledge that is translatable from mice to humans to add to the knowledge necessary for setting standards for radiation protection and ease concerns about radiation exposure at low doses.

Acknowledgements

I would first like to thank my supervisor Dr. Simon Lees for this opportunity. I had no idea what I was getting into accepting a spot in your lab group but it was the best decision I could have made. Your door was always open when I needed help and you never missed out on a teaching moment. I have learned an exceptional amount in the last two years and I could not have done it without your help. I could not have imagined having a better mentor for my Masters. To my co-supervisor, Dr. Neelam Khaper. Thank you for always being available when I had questions and providing useful insight. You have taught me that I should always push the limits and strive to make my work exceptional. A sincere thank you to my committee member, Dr. David Law, for your patience and insightful comments. Your questions prompted me to go back to the basics and look at the big picture.

To Sarah Niccoli, you are the heart and soul of the Lees Lab. You invested your time to train me and I would not be where I am without you. I can't thank you enough for your patience when answering my endless questions, friendship, and all the laughs along the way. There was never a dull moment.

I thank my fellow labmates at NOSM for making my time in and out of the lab enjoyable especially those of you that I spent long days with at Munro. To my friends and fellow grad students, thank you for reminding me that taking a break from school is necessary. I hope our friendship spans far into the future regardless of where our schooling and jobs may take us.

Finally, I am grateful to my parents and family members for their love and encouragement throughout this journey especially during stressful moments. The retail therapy really helped. A big thank you to my Nan for letting me stay at her house on multiple occasions so I could be close to the lab and inviting me for lunch almost every day of the week. I would not have been able to do this without you.

Table of Contents

List of Figures

List of Tables

Chapter 1. Introduction

1.1 Statement of Problem

Exposure to ionizing radiation and the possibility of radiation contributing to negative health outcomes is a widespread concern. The public, scientific community, and workers, specifically in the nuclear energy industry and diagnostic imaging, are exposed to different sources of radiation. Pregnant women represent a vulnerable group and are sometimes exposed to radiation during diagnostic imaging if the woman is not aware of the pregnancy or in emergency situations. Effects of exposure on the fetus are dependent on gestational age and absorbed radiation dose. The fetal programming hypothesis which states that an adverse in-utero environment or stress during development of an embryo or fetus can result in permanent physiologic changes [1], which often result in progressive metabolic dysfunction with age.

The body uses glucose as a main source of energy. Glucose metabolism must be tightly regulated to maintain proper organ function. In response to postprandial glucose, β-cells in the pancreas sense changes in plasma glucose levels and release the hormone insulin, stimulating glucose uptake and metabolism in adipose tissue and liver [2].

In the liver, insulin binds to insulin receptors leading to cell signaling events that regulate glucose metabolism. Insulin stimulates glucose uptake, glycogenesis, and glycolysis while inhibiting the production of glucose through gluconeogenesis and glycogenolysis [2]. Glucose and lipid metabolism are closely related. Alterations in glucose metabolism can lead to insulin resistance, a condition where β-cells in the pancreas produce insulin in response to glucose but cells are unable to respond to the insulin effectively leading to hyperglycemia. This can be caused by defects in the insulin signaling pathway. Type 2 diabetes, obesity, and non-alcoholic fatty liver disease are associated with insulin resistance [3]. An alternative energy source for the liver, in times of glucose deficiency, are triglycerides which have been stored through lipogenesis [4]. However, accumulation of hepatic or circulating triglycerides from an imbalance

in de novo lipogenesis/lipid uptake and lipid disposal leads to adiposity which is linked to obesity and metabolic syndrome [5], [6].

The role of brown adipose tissue (BAT) in energy homeostasis and metabolism is a growing area of interest after advancements in technology have identified BAT in adult humans. It was originally thought to be present only in infants and small animals. BAT is responsible for non-shivering thermogenesis through uncoupling protein 1 (UCP1) which uncouples oxidative phosphorylation resulting in heat production rather than ATP formation [7]. Recently, BAT has been identified as an endocrine organ with a role in regulating metabolism [8]. Transplant studies have shown that increasing the amount of BAT in rodents results in increased glucose uptake and improved insulin sensitivity in endogenous BAT, white adipose tissue and the heart [9]. In humans, the amount of BAT is inversely related to body mass index (an indicator of obesity) [10], [11].

1.2 Significance of Study

There are several established models of fetal programming that induce in-utero stress including maternal undernutrition, protein-restricted diets, maternal obesity, prenatal hypoxia, and exposure to stress hormones like glucocorticoids. These models present similar outcomes with the offspring demonstrating alterations in birth weight followed by weight normalization within the first few months. Intrauterine growth restriction and low birth weight seem to predispose offspring to insulin resistance and impaired glucose metabolism [12]–[14]. Glucocorticoid exposure, maternal obesity, and maternal undernutrition or diet restriction predispose animals to alterations in metabolism and insulin resistance [15]–[18]. Prenatal hypoxia contributes to cardiovascular disease development in adulthood [19]. Maternal obesity fetal programming models are associated with offspring insulin resistance and increased adiposity [20]. Overall, a poor maternal state leads to placental insufficiency and negative health outcomes of the offspring.

Diagnostic radiation exposure may be a potential cause of increased cancer risk [21]. Moreover, pregnant women represent a more vulnerable population [22]. The effect of radiation on the fetus has been studied through animal studies and from atomic bomb exposure [23]. Radiation exposure in the third trimester of pregnancy, has been reported to result in behavioural, social, and locomotor changes in the offspring in adulthood as well as the appearance of microcephaly [24], [25]. However, little is known about the effects of sub-lethal dose radiation (SLDR) on fetal programming of glucose metabolism and glucose uptake. Alterations to metabolism at young age are thought to contribute to severe metabolic dysfunction in later life. First, we must understand the impact of radiation in sub-lethal doses to understand the risks for various exposures.

1.3 General Research Question

Does SLDR exposure in the third trimester of pregnancy alter glucose metabolism of the offspring?

1.4 Specific Aims

1. Determine the effects of SLDR on glucose metabolism in the liver.

Rationale:

Insulin sensitive tissues such as the liver are susceptible to insulin resistance. Alterations in hepatic glucose metabolism can lead to impaired whole body glucose metabolism, insulin resistance, type 2 diabetes, obesity, and metabolic syndrome. Low birth weight is predictive of insulin resistance. Stress models of fetal programming have shown increases in gluconeogenesis and increases in protein expression of proteins involved in gluconeogenesis when offspring had low birth weights [29], [30]. Radiation presents a stress event that may have similar affects. Measuring the expression of proteins in the liver associated with insulin resistance such as suppressor of cytokine signaling 3

(SOCS3) and phosphoenolpyruvate carboxykinase (PEPCK), can indicate alterations in hepatic glucose metabolism.

Hypotheses:

SLDR will cause alterations in glucose metabolism and an accumulation of hepatic triglycerides in offspring.

2. Determine the effects of SLDR on interscapular brown adipose tissue (IBAT) glucose uptake *in vivo.*

Rationale:

BAT activity is linked to increased energy expenditure, glucose utilization from the bloodstream and stored lipid use. In BAT, glucose uptake indicates metabolically active tissue. IBAT glucose uptake can be measured *in vivo* using microPET imaging with ^{18}F-fluorodeoxyglucose (^{18}F-FDG). A compensatory increase in BAT activity is observed in fetal programming models of protein restriction [26]. Plasma triglyceride levels have been shown to decrease with increased BAT activity [27], [28].

Hypotheses:

SLDR will cause an increase in IBAT glucose uptake to compensate for impaired whole-body glucose metabolism. SLDR will also decrease plasma triglycerides.

3. Determine the effects of SLDR on cell signaling in BAT.

Rationale:

BAT is regulated by insulin signaling, however, it seems that BAT activity is primarily regulated via β-adrenergic signaling [31]–[34]. Studies have reported that BAT activity can be restored or enhanced by using β-adrenergic receptor agonists [32], [34]. Data from our laboratory, observed majority of basal BAT

activity to be β-adrenergic mediated but it is responsive to insulin. By looking at targets from each of the pathways, we can determine the method of action leading to alterations in glucose uptake. Protein kinase B (Akt) will be used as an insulin signaling pathway target. Glycogen synthase kinase 3 beta (GSK3β) is involved in both the β-adrenergic signaling and insulin signaling pathways. By combining the data for Akt and GSK3β protein expression and phosphorylation status, the pathway responsible for the increased glucose uptake in IBAT can be suggested. BAT activity can also be measured by UCP1 expression as increased UCP1 is an adaptation to chronic BAT activity [26].

Hypotheses:

Exposure to SLDR will result in an increase in the phosphorylation of GSK3β but no change in the phosphorylation of Akt suggesting increased BAT activity is a result of increased β-adrenergic signaling. SLDR exposure will result in an increase in UCP1.

Chapter 2. Literature Review

2.1 Fetal Programming

Environmental effects in-utero have long term influences on health outcomes in later life. The fetal programming hypothesis describes the concept that adult disease can originate from in-utero programming during development when internal or external environmental conditions are suboptimal [1]. This results in permanent physiologic changes that lead to progressive metabolic dysfunction with age [1]. Stress events cause a fight-or-flight response in the mother that trigger the hypothalamic-pituitary-adrenal (HPA) axis to produce hormones capable of crossing the placenta and affecting the fetus [35]. Stress is thought to cause permanent modification of the HPA axis [36]. Xiong and Zhang 2013, review the role of the HPA axis and how alteration in its activity can be detrimental to the fetus and affect developmental processes [37]. That means fetal growth and development are dependent on the mother's nutritional, hormonal, and metabolic environment.

Epidemiological studies have consistently shown a relationship between high or low birth weights and development of disease in adulthood [38], [39]. Low birth weight can occur because of preterm delivery or intrauterine growth restriction (IUGR) caused by substrate limitation to the embryo or fetus. The thrifty phenotype hypothesis links poor fetal and infant growth to changes in glucose metabolism leading to increased risk of metabolic disorders such as metabolic syndrome and type 2 diabetes [40], [41]. Studies focusing on maternal obesity and high-fat diets have found that elevated birth weight offspring are also at risk [39], [42]. Fetal programming has been demonstrated in several species, including sheep, baboons, guinea pigs, rats, and mice, using a range of techniques to induce alterations in offspring birth weight including exposure to stress hormones, maternal diet, and maternal environmental stressors.

2.1.1 Models of Fetal Programming

2.1.1.1 Maternal Nutrition

The fetus responds to poor maternal nutrition from maternal protein restriction or undernutrition by activating adaptive processes. Undernutrition is associated with obesity, insulin resistance, and type 2 diabetes [43]–[45]. Similarly, models of maternal nutritional excess, like high-fat diets, lead to an offspring phenotype that resembles metabolic syndrome with impaired glucose metabolism, increased plasma triglycerides, and increased adiposity [46], [47]. Offspring of obese dams that continue to consume a high-fat diet display features of metabolic syndrome and have increased lipid accumulation in the liver [48], [49]. Metabolic effects are more pronounced in female offspring [49]. These offspring are more likely to develop insulin resistance in later life, and more likely to give birth to overweight babies.

2.1.1.2 Prenatal Hypoxia

Prenatal hypoxia is a model of fetal programming where the fetus lacks the appropriate level of oxygen required for development. This can be caused by the mother travelling to high altitudes, or conditions like pre-eclampsia [50]. Risks are higher when exposure occurs in the second and third trimester of pregnancy because the early stages of pregnancy occur under anaerobic conditions anyway [19]. The main consequence of prenatal hypoxia in humans and rodents appears to be IUGR [51]–[53]. The fetus does not grow to its full potential and is born small for their gestational age leading to early onset of adult diseases.

2.1.1.3 Stress Hormones

Cortisol is a glucocorticoid hormone important for development and maturation in late gestation. Glucocorticoids control the HPA axis, a negative feedback loop that stimulates glucose metabolism, promotes fatty acid release, and inhibits protein synthesis [54], [55]. Stress models of fetal programming use excess endogenous or synthetic glucocorticoids, such as dexamethasone or

betamethasone, which permanently alter HPA axis function [36]. Fetal exposure to glucocorticoids are thought to alter the function of the HPA axis and to contribute to insulin resistance in later life [29]. Dexamethasone is known to cause IUGR and glucose intolerance in adult offspring [29]. Changes are also seen in the liver and in circulating levels of leptin, insulin, and corticosterone [29]. While hepatic glycogen content and glycogen phosphorylase expression remain unchanged, overexpression of hepatic gluconeogenic enzyme phosphoenolpyruvate carboxykinase (PEPCK) is frequently observed and thought to be responsible for increasing gluconeogenesis [29], [56].

2.1.1.4 Radiation Exposure

There is a lack knowledge on the effects of low dose radiation (LDR) or sub-lethal dose radiation (SLDR) on fetal programming of metabolism. What is known comes from animal studies and the aftermath of the atomic bombs and measures are limited to small head size observed in children, intelligence quotients, and behavioural and locomotor changes observed as adults [23], [57]–[60]. Mechanisms of how LDR and SLDR effect the fetus remain unknown.

2.2 Ionizing Radiation Exposure

Radiation is classified as ionizing or non-ionizing. Non-ionizing radiation sources include ultraviolet (UV) rays from the sun or tanning beds, and electromagnetic radiation from radio waves and microwaves [61]. Ionizing radiation has more energy than non-ionizing radiation, enough to remove electrons from an atom. Ionizing radiation can be direct, caused by alpha or beta particles, or indirect, caused by gamma rays or X-rays [61]. Gamma and X-rays are more penetrating and can cause more biological damage. Damage can include inducing oxidative stress resulting in DNA methylation, DNA bond breakage, or post-translational histone modifications [61]. These modifications can affect gene expression profiles that may lead to either adaptive processes

or progression of disease reviewed in more detail by Tharmalingam et al. 2017 [62], and Lee 2015 [63].

2.2.1 Radiation Exposure in Humans

The Canadian Nuclear Safety Commission's Radiation Protection Regulations sets an annual dose limit of 1 mSv for the public and 50 mSv for nuclear energy workers [64]. Table 1 summarizes the health effects and limits at certain absorbed radiation doses. Responses to radiation can vary between individuals based on radiation source, radiation dose, length of exposure, and genetic makeup. High doses of radiation are rare outside of radiotherapy and nuclear disasters whereas low dose radiation exposure is much more common [65]. Less is known about the outcomes from LDR exposure. LDR can come from occupational exposures, diagnostic imaging, cancer therapy, natural areas of high background (radon), and space travel (airplanes). The existing guidelines attempt to limit the exposure of workers in nuclear and medical industries but there is still concern. Scientific evidence of risks and/or benefits from LDR are lacking. Linear no-threshold model has been used to extrapolate detrimental health effects in humans from LDR, less than 100 mSv [66]. Extrapolation from high-dose effects may not necessarily reflect the biological outcomes at low doses. For example, the model doesn't account for biological defense mechanisms that could repair damage done by radiation [66].

Table 1. Health effects and limits of radiation from the Canadian Nuclear Safety Commission [67].

Dose (mSv)	Health Effect or Limit in Humans
Greater than 5000	May lead to death when received all at once
1000	May cause symptoms of radiation sickness if received within 24 hours
100	Lowest acute dose known to cause cancer
30-100	Radiation dose from a full body CT scan
50	Annual radiation dose limit for nuclear workers
1.8	Average annual Canadian background exposure
1	Annual public radiation dose limit
0.1-0.12	Dose from lung X-ray
0.01	Dose from dental X-ray, average annual dose due to air travel

Radiation is commonly measured in gray (Gy) which is a unit of absorbed dose reflecting the energy distributed into the mass of tissue or sieverts (Sv) which is the biological equivalent dose, taking into account the amount and type of radiation. 1000 mSv is equal to 1000 mGy.

The possibility exists that exposure to low dose radiation may be beneficial. Studies have shown that exposure to doses less than 100 mGy act as a primer and may have protective effects on subsequent high dose radiation exposure [68], [69]. Without more evidence of the benefits from LDR in humans, there remains concern over the perceived increased risk of developing cancer.

2.2.2 Radiation Exposure in Mouse Models

Compared to humans, mice require a higher radiation dose for similar health effects to be observed. Animal studies on ionizing radiation have categorized doses of radiation as ultra-low, low, and high. Ultra-low radiation is characterized as a dose less than 1 mGy. United Nations Scientific Committee on the Effects of Atomic Radiation classifies low dose radiation as any dose below 100 mGy [70]. High doses vary significantly ranging from 2000 mGy to

50,000 mGy. The higher doses are usually accumulated during multiple exposures over time rather than a one-time whole-body exposure.

There are major differences in mouse strain radiation sensitivity. Radiation sensitivity is referenced as LD50:30 which is the dose of whole-body radiation that is lethal to 50% of the target population by 30 days after exposure. Grahn and Hamilton 1956, demonstrated C57Bl/6 mice to have an LD50:30 of 6300 ± 40 mGy and consider this strain to be radioresistant [71]. In comparison, BALB/c mice are considered radiosensitive with an LD50:30 of 5000 ± 60 mGy. In humans, the LD50:30 is approximately 4500 mGy [72]. With this knowledge, the amount of radiation can be adjusted to be comparable to the doses and physiological risks in humans. For the present study, a dose of 1000 mGy was chosen for C57Bl/6J mice. This dose is frequently used in LDR studies when looking at a dose response as a comparable high dose (Table 2). Rather than attempting to classify 1000 mGy as high or low dose, for the purposes of this study, 1000 mGy will be considered a sub-lethal dose.

2.2.3 Radiation Exposure During Pregnancy

Pregnant women represent a population that is more vulnerable to radiation exposure. There is concern for both the mother and the unborn child. The risks of prenatal exposure to ionizing radiation are dependent on the absorbed dose and timing of exposure related to gestational age [21], [73], [74]. During the first trimester, radiation risks are most significant. High doses of radiation exposure during the pre-implantation stage can result in failure to implant leading to abortion. Russel (1950) studied radiation at doses of 1000-4000 mGy during the pre-implantation stage (days 0-5 of gestation) in pregnant mice and found an “all-or-nothing” effect where the doses were either lethal or had no effects at all [75], [76]. If the embryo survives the exposure, it will likely fully develop and have low risk of congenital abnormalities. It is generally accepted that exposures to low doses during the first two weeks of pregnancy may cause damage that can be compensated for or repaired [77], [78]. Low doses are detrimental during organogenesis (weeks 2 – 8). There are

increased risks of malformations, growth restriction, and behavioural or motor skill deficits discussed by De Santis et al. 2007 [79]. Radiation risks are somewhat less in the second trimester [80]. The third trimester, or late gestation, is a critical stage where cells can be influenced by changes in the in-utero environment resulting in adaptations in cellular function [81]–[83].

2.2.4 Prenatal Radiation Exposure in Humans

High dose ionizing radiation exposure is known to be mutagenic and carcinogenic. Health effects from high dose radiation exposure in humans are documented from events like the Chernobyl disaster and the atomic bombings of Hiroshima and Nagasaki. Data for prenatal exposures comes predominantly from survivors of the atomic bombs that were pregnant at the time and within 2000 metres of the hypocenter. Individuals closer to the hypocentre at the time of the explosion received higher radiation doses and negative health effects were more common [84], [85]. Fetal exposure doses were estimated from this information. Reports show children that were exposed in-utero have increased incidence of mental impairments marked by reductions in intelligence quotient score based on informed clinical opinion, microcephaly, growth restriction, and childhood thyroid cancer [84], [86], [87]. From these cases, microcephaly and mental impairments appear to be independent of each other. Reports of microcephaly are higher when the exposure occurred during the first and second trimester compared to third trimester [86].

Less is known about the effects of LDR exposure. Several studies suggest negative health effects from LDR exposure from medical diagnostic imaging like computed tomography scans [88], [89]. There is evidence of a positive relationship between long term exposure to LDR and leukemia [90]. But there are limitations to these studies and as such require further exploration to understand the full effect of LDR on humans and animals. Another factor to consider when conducting these studies is that the dose delivered to the fetus is thought to be lower than what the mother is exposed to and likely falls below the threshold dose for deterministic effects [91]. With

limited data available for LDR exposure in humans, researchers have turned to animal models to assess radiation effects.

2.2.5 Prenatal Radiation Exposure in Rodent Models

Mouse models require higher radiation doses than humans to produce similar morphological and physiological changes. The short life span of mice makes it easy to track changes of long-term effects. Like humans, the day of radiation exposure during gestation is important. Studies have found that irradiation on day 14 of gestation is high risk for locomotor function and behavioural changes [92], [93]. The brain is developing during the third trimester and therefore, radiation exposure during gestation day 13-18 has detrimental effects on the brain [93]. Day of experiment to test changes is important because some effects exist at an early age and become unobservable later in life or vice versa. Behavioural changes in mouse models initially measured at 6 months of age appear to persist to 12 months but are no longer observed at 18 months old [94]. Chromosomal instability was observed in bone marrow at doses of 500 mGy and higher at 12 months old and has been suggested as a mechanism for the progression of leukemia [95]. In majority of LDR studies, health affects get worse around 12 months of age and disappear by 18 months (Table 2).

Dose response relationships are observable for brain weight, body weight, behavioural changes, learning function, and memory retention [92]–[94], [96], [97]. Other stressful events, like restraining the animal while irradiating without the use of anesthesia, could have induced changes presumed to be from radiation. Effects of gamma radiation at doses of 100 to 3000 mGy in mouse models are summarized in Table 2. While there is evidence of neurological and behavioural changes, there is no data available for the effects of LDR on metabolism and physiological changes.

Table 2. Prenatal ionizing radiation exposure from gamma radiation in mouse models (Gestation day 14-17).

Mouse Strain	Day of Irradiation	Type of Radiation	Dose (mGy)	Age at time of testing	Health Effects	Reference
Male C57BL/6 X C3H Hybrid	14	^{137}Cs gamma radiation	100, 200, 500, 1000	6-7 months; 12-13 months; 19-20 months	Increased spontaneous circadian motor activity suggesting nocturnal hyperactivity in young and adult mice irradiated at 1000 mGy.	[98]
Male C57BL/6 X C3H Hybrid	14	^{137}Cs gamma radiation	1000, 2000, 3000	6 months	Dose related decrease in body and brain weight. Dose related increase in superior colliculi area.	[96]
Male C57BL/6 X C3H Hybrid	14	^{137}Cs gamma radiation	500, 1000	6-7 months; 12-13 months; 19-20 months	Behavioural changes at 19-20 months.	[99]
Swiss albino	17	^{60}Co gamma radiation	300, 500, 1000, 1500	6 months	Learning and memory function impairment. Dose dependent decrease in brain weight.	[97]
Swiss albino	17	^{60}Co gamma radiation	300, 500, 1000, 1500	6 weeks	Increased mortality and growth restriction at doses ≥1000 mGy.	[100]
Swiss albino	14	^{60}Co gamma radiation	250, 300 500, 1000, 1500	6, 12, 18 months	Behavioural changes at 300 mGy and higher. Linear dose response. Changes persisted at 12 months but not significant at 18 months.	[94]

Swiss albino	14, 17	^{60}Co gamma radiation	250, 500, 1000, 1500	6, 12 months	Decrease in brain weight. Decrease in neuron number in regions of the hippocampus.	[93]
Swiss albino	14, 17	^{60}Co gamma radiation	250, 500, 1000, 1500	12 months	Low peripheral blood count. Dose dependent increase in abberant metaphases in bone marrow. Radiation induced genome instability.	[95]
Swiss albino	14	^{60}Co gamma radiation	250, 500, 1000, 1500	6, 12, 18 months	Dose-dependent decrease in learning ability and memory retention at 6 months at doses >250 mGy. Changes persistent to 18 month at doses ≥500 mGy.	[92]

Overall, there is no consensus on what is a high versus low dose of radiation when it comes to fetal programming. The dose of absorbed radiation from a whole-body exposure by the mother may not be the same as the dose that reaches the fetus. Negative or positive effects of SLDR in animal models may elucidate mechanisms responsible for LDR fetal programming in humans and provide information for prevention or therapeutic intervention.

2.3 Brown Adipose Tissue

2.3.1 Characteristics and Function

Until recently, brown adipose tissue was thought to be present in only neonates and young children who were not capable of shivering to maintain core body temperature upon cold exposure and rely on non-shivering thermogenesis of BAT to keep warm. With age, it was thought BAT would transform into white adipose tissue (WAT), responsible for storing energy in the form of lipids and

making up majority of human adipose tissue. With the advancement of positron emission tomography (PET) imaging and development of radioactive tracer ^{18}F-fluorodeoxyglucose (^{18}F-FDG), BAT was detected in adult humans supplementing Heaton's biopsy findings from 1972 [10], [101]. In humans, BAT is distributed symmetrically in the neck (cervical-supraclavicular), along the spine (paravertebral), in the chest around the heart (mediastinal), and by the kidneys (perirenal) (Figure 1A) with higher prevalence in females than males [102]. In rodents, BAT depots are found in the interscapular, subscapular, axillary, perirenal, and periaortic regions (Figure 1B) [103]. The interscapular region is the most accessible depot in mice making it the region of choice for most animal studies.

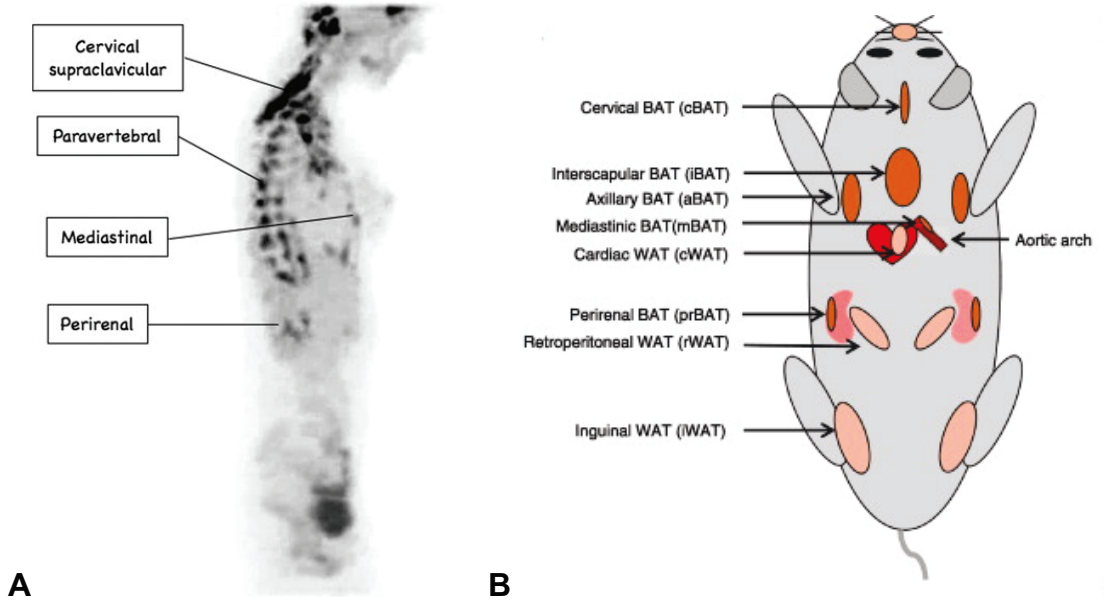

Figure 1. Brown adipose tissue depots. (A) Human brown adipose tissue is located in cervical-supraclavicular, interscapular, paravertebral, and mediastinal regions. Image from Richard et al. 2010 [104]. (B) Rodent brown adipose tissue depots are located in the interscapular, subscapular, axillary, perirenal, and periaortic regions. Image taken from Vosselman et al. 2013 [103].

Both human and rodent BAT is characterized by brown adipocytes that contain multilocular lipid droplets densely packed with mitochondria, rendering the tissue brown in colour. The mitochondria contain uncoupling protein 1 (UCP1), a protein found in BAT but not in WAT, which uncouples oxidative phosphorylation resulting in heat production, rather than ATP formation (Figure 2) [105]. UCP1 allows the transfer of protons from the intermembrane space into the mitochondrial matrix dissipating the proton gradient necessary for the phosphorylation of ADP to ATP [106].

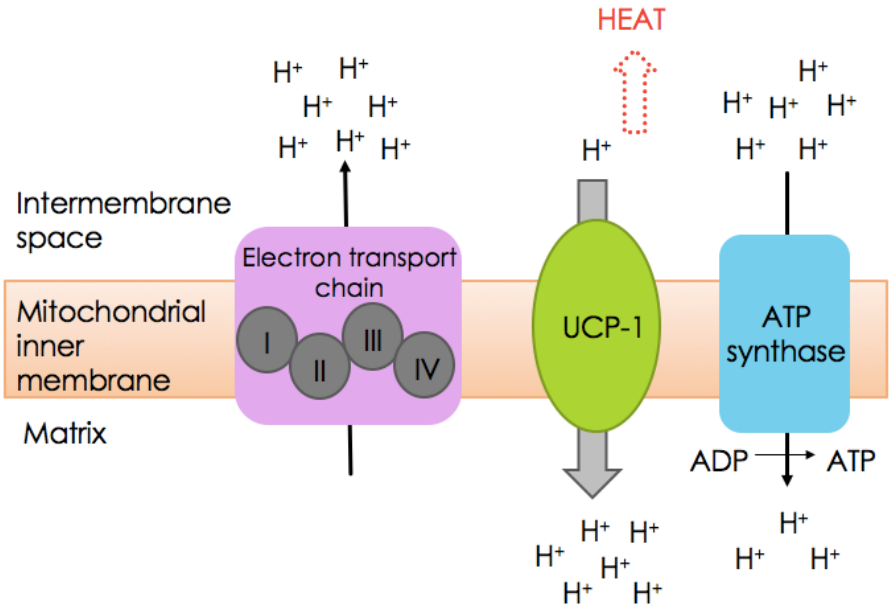

Figure 2. Uncoupling protein 1 (UCP1). UCP1, a protein found in BAT, is responsible for heat production through non-shivering thermogenesis. Located in the mitochondrial inner membrane, the electron transport chain generates a proton gradient that drives ATP synthesis. Uncoupled oxidative phosphorylation through UCP1, brings protons back into the mitochondrial matrix to dissipate the proton build up in the intermembrane space. Heat is produced as a by-product. Numbers I-IV correspond to electron transport chain complexes with ATP synthase as the fifth complex. Figure adapted from Richard and Picard [107].

UCP1 is activated and expression is increased by the β-adrenergic pathway (Figure 3). UCP1 activation also requires the binding of fatty acids but this mechanism remains contentious [108]–[111]. It is known that β3-adrenoreceptor agonists induce UCP1 expression and thermogenesis in rodents and isolated brown adipocytes [108], [112]–[114]. β3-adrenoreceptor agonists also enhance glucose metabolism in rodents [32], [115]. UCP1 null mice are not able to maintain their body temperature when exposed to the cold and develop an obese phenotype at thermoneutral temperature [116].

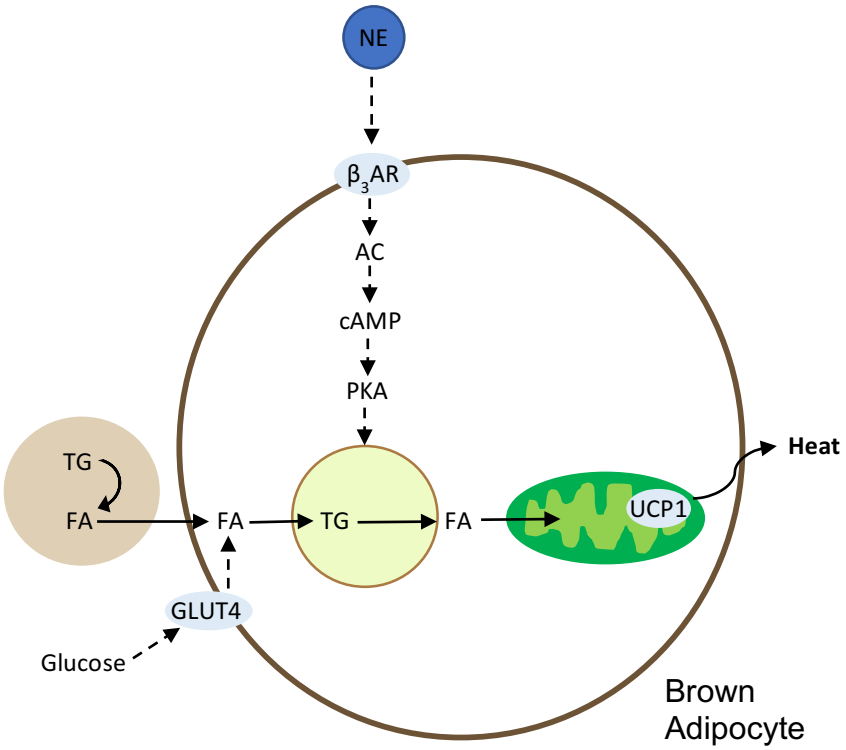

Figure 3. UCP1 is activated in brown adipocytes by β-adrenergic signaling. Norepinephrine binds to β3-adrenoreceptors at the cell membrane of brown adipocytes triggering a signaling cascade stimulating cyclic adenosine monophosphate (cAMP) production. cAMP activates protein kinase A (PKA) which stimulates lipolysis. Adipocytes take up fatty acids derived from intracellular triglycerides and glucose and form lipid droplets. Fatty acids are

released from lipid droplets and combusted by the mitochondria or bind allosterically to activate UCP1. Adapted from Kooijman et al. 2015 [117].

Evidence from transplant studies have shown BAT to have a role as an endocrine organ releasing endocrine factors, or adipokines, including insulin-like growth factor 1, fibroblast growth factor 21, interleukin 6, and neuregulin 4 that target peripheral tissues such as WAT, liver, pancreas, and bone. A review focused on the adipokines released by BAT can be found in Villarroya et al. [8] as it will not be covered here.

2.4 Metabolism

2.4.1 BAT Metabolism

BAT is highly vascularized and innervated by the sympathetic nervous system [108], [118]. Its activation is predominantly controlled by β-adrenergic signaling [108]. Non-shivering thermogenesis is controlled by the hypothalamus where in response to overfeeding or cold exposure, the sympathetic nervous system releases norepinephrine which binds to β_3-adrenergic receptors, the most significant type of β-adrenergic receptor in mature brown adipocytes (Figure 3) [108]. This results in the activation of its G-coupled protein. Subsequently, adenyl cyclase stimulates the formation of cyclic adenosine monophosphate (cAMP) [108]. cAMP activates protein kinase A (PKA) resulting in (1) enhanced synthesis of UCP1 (a marker of thermogenesis), (2) increased intracellular lipolysis, and (3) phosphorylation and inhibition of glycogen synthase kinase 3 beta (GSK3β). GSK3β inhibition will reduce phosphorylation of glycogen synthase decreasing glycogen synthesis.

BAT is an insulin sensitive tissue meaning that it can also be controlled by the insulin signaling pathway [119]. Insulin binds to an insulin receptor at the plasma membrane inducing a conformational change that leads to the phosphorylation of tyrosine residues in the β subunit (Figure 4). The residues are recognized by insulin receptor substrates (IRS). Activation of the receptor

leads to phosphorylation of tyrosine residues on the IRS proteins that are recognized by phosphatidylinositol 3-kinase (PI3K). This leads to a signaling cascade that results in protein kinase B (Akt) translocating to the plasma membrane where it is activated by phosphorylates. Akt will subsequently phosphorylate and inhibit GSK3β decreasing glycogen synthesis [120]. GSK3 activity is increased in skeletal muscle and adipose tissue in insulin resistance states [121], [122].

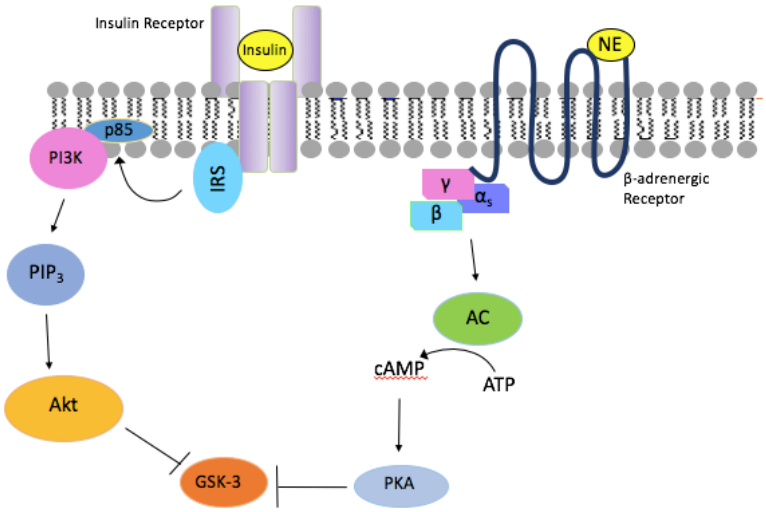

Figure 4. BAT pathways. BAT is controlled by two pathways: β-adrenergic and insulin signaling pathways. Norepinephrine binds to a β-adrenergic receptor resulting in a signaling cascade that increases cyclic adenosine monophosphate (cAMP) and eventually leads to the phosphorylation and inhibition of glycogen synthase kinase 3 beta (GSK3β). Insulin binds to the insulin receptor beginning a signaling cascade that results in protein kinase B (Akt) phosphorylating and inactivating GSK3β.

BAT can be activated when body temperature decreases or after consuming food [123], [124]. BAT uses glucose, intracellular triglycerides and free fatty acids from circulation to generate heat to protect against cold exposure and burn excess energy to prevent adiposity (Figure 3) [125]. Its activation leads

to increased energy expenditure, increased glucose uptake, insulin sensitivity, and a decrease in body weight and triglycerides [27]. Therefore, BAT is becoming increasingly recognized as a target for obesity and diabetes treatments [126]. BAT transplantation studies found that increasing the amount of BAT present in mice, increased whole-body and tissue glucose metabolism by improving glucose uptake into endogenous BAT, WAT, and heart muscle [9].

2.4.2 Liver Metabolism

Understanding normal hepatic glucose metabolism is important for recognizing metabolic alterations that can result from fetal programming. The liver, along with skeletal muscle, is a main site of glucose utilization after a meal. Food is digested in the gastrointestinal tract, and glucose, fatty acids, and amino acids are absorbed into the bloodstream and transported to the liver through the portal vein [2]. Glucose enters liver hepatocytes via GLUT2 transporters located at the plasma membrane. Once in the hepatocytes, glucose can (1) enter the glycolytic pathway to form ATP, (2) enter the glycolytic pathway to be used in fatty acid and triglyceride synthesis in a process called lipogenesis, or (3) be stored as glycogen, a process called glycogenesis. Glucose not entering the liver on first pass via portal vein goes to other tissues like skeletal muscle.

The liver is responsible for maintaining normal blood glucose levels. Liver metabolic activity is tightly regulated by hormones like insulin. In response to high blood glucose levels, or in fed-state, β-cells in the pancreas release insulin into the bloodstream stimulating glucose uptake, glycolysis, lipogenesis, and glycogenesis. Insulin will inhibit the production of glucose by gluconeogenesis and glycogenolysis. Alternatively, when blood glucose levels are low and glycogen stores have been depleted, a non-carbohydrate source, like amino acids, can be converted into glucose through gluconeogenesis.

Alterations to any of these pathways can lead to insulin resistance, impaired whole-body glucose metabolism, type 2 diabetes mellitus, or metabolic syndrome [127], [128]. Insulin resistance occurs when the tissue no longer responds to insulin [129]. In the liver, insulin resistance has a collective response

involving the increase of gluconeogenesis and glycogenolysis and the reduction of glucose uptake and glycogen synthesis. This can lead to hyperglycemia, having blood glucose levels above the normal range. Insulin resistance increases the risk of developing type 2 diabetes mellitus and is also a symptom of metabolic syndrome along with high blood pressure, abdominal obesity, and abnormal triglyceride and cholesterol levels [130].

The liver is involved in many pathways of lipid metabolism. Fatty acids are obtained from absorption of dietary fats, from lipolysis in adipose tissue, or de novo synthesis in the liver [4]. Once in the liver, fatty acids can be oxidized for energy, converted to triglycerides for storage or secreted as very-low density lipoprotein [2]. Like glucose metabolism in the liver, lipid metabolism is a tightly controlled process, that includes import of lipids into the liver, and lipid oxidation or export, to maintain the appropriate balance in the liver.

Situations where triglycerides or fatty acids accumulate in the liver due to an imbalance in lipid storage and removal can be an indicator of disease or dysfunction [131]. Accumulation of lipids, which form droplets in the liver, is called hepatic steatosis. Chances of developing hepatic steatosis increase with age [132]. Hepatic lipid accumulation has been linked to insulin resistance [133]. Hepatic steatosis can progress into more serious diseases including non-alcoholic fatty liver disease or non-alcoholic steatohepatitis.

2.6 Positron Emission Tomography

2.6.1 Principle of PET imaging

PET is an imaging modality that detects the emission of high-energy photons emitted from radiotracers. PET has a purpose in both research and clinical settings. It begins with a proton-rich isotope that decays to a neutron, a positron and a neutrino. The positron emitted travels a short distance through tissues before it reaches an electron in the tissue. The particles combine and “annihilate” each other resulting in the emission of two coincidence gamma ray photons (Figure 4). Each of the resulting photons has an energy of 511keV.

Detectors are usually arranged in a ring to simultaneously detect the two gamma rays and from there a computer converts the signals into detailed pictures for analysis.

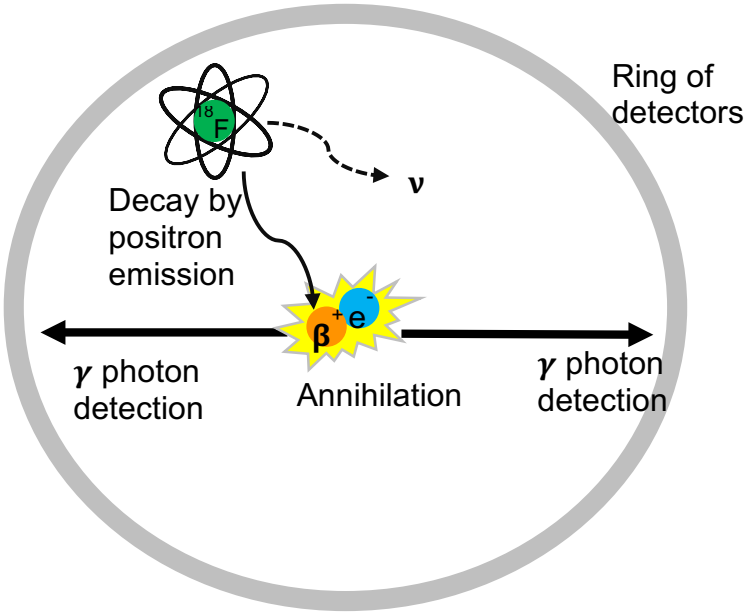

Figure 5. A representation of the principle of PET imaging. The radiotracer isotope decays releasing a neutron, a positron (β+), and a neutrino (ν). The positron collides with an electron in the tissue and they annihilate producing two gamma ray photons that can be read by a ring of detectors. Image adapted from Miller et al. 2008 [134].

2.6.2 PET Radiotracer – ^{18}F-FDG

^{18}F-FDG is commonly used in animal research and clinical settings to assess tissue specific glucose metabolism. ^{18}F-FDG possesses several ideal characteristics for a radiotracer including a short positron range and half-life of 109.8 minutes allowing sufficient time to image, but is not long enough to cause prolonged radiation exposure. ^{18}F is a proton rich isotope that replaces a hydroxyl group at position C-2 on a deoxyglucose molecule. Deoxyglucose is a glucose analogue that can be taken up by glucose transporters. Therefore, ^{18}F-FDG is taken up by any tissue in the body that utilizes glucose. Once inside the

cell, ^{18}F-FDG is phosphorylated by hexokinase to FDG-6-phosphate. The phosphorylated metabolite is no longer a substrate for GLUT1 or 4, cannot be metabolized further, and accumulates in the cell. In the presence of glucose-6-phosphatase, FDG-6-phosphate can be dephosphorylated and leave the cell but this happens slowly as the amount of glucose-6-phosphatase is limited. The liver is one exception; it has more glucose 6-phosphatase than other tissues allowing the tracer to evacuate the cells and prevents accumulation of the tracer [135]. The amount of tracer present in a tissue is proportional to glucose uptake. Metabolically active tissues will take up glucose. ^{18}F-FDG was originally used in oncology for the identification of cancer cells which have increased glucose metabolism as reviewed in an article by Almuhaideb et al. 2011 [136]. It can also be used to measure physiological glucose uptake or response to treatment in the heart, brain, BAT, muscle, bladder, liver and kidneys and allow for visualization of interaction between the organs.

2.6.3 ^{18}F-FDG PET for Tissue Specific Glucose Uptake in IBAT

PET imaging with ^{18}F-FDG was pivotal in the discovery of BAT in humans. Now, ^{18}F-FDG uptake is used to measure metabolic activity. Initially, it was commonly used to indirectly measure thermogenesis but recent findings suggest that the stimulation of β-adrenergic signaling can increase ^{18}F-FDG uptake independent of UCP1 thermogenesis [56], [137], [138]. In one contradictory study, female UCP1 knock-out mice were used in an experiment with β-adrenergic agonist, CL316243, that observed ^{18}F-FDG uptake to be unaffected when compared to wild-type mice [56]. On the other hand, in male UCP1 knock-out mice, β-adrenergic stimulated activation was dependent on the presence of UCP1 [139].

Other factors that affect ^{18}F-FDG uptake in human BAT are sex, age, BMI, and environmental temperature. Regions of active BAT marked by ^{18}F-FDG uptake are more prevalent in females than males [10]. ^{18}F-FDG uptake in BAT is also dependent on age where younger individuals demonstrate higher uptake than older individuals [140]. Lower outdoor temperatures, measured

monthly, increased BAT glucose uptake [140]. ^{18}F-FDG has an inverse relationship to BMI [141]. The final factor that can affect ^{18}F-FDG uptake in BAT is insulin sensitivity. Cold-stimulated glucose uptake in BAT is reduced in insulin-resistant states like diabetes [142]. More information is needed to find out if diabetes is responsible for the decrease in BAT glucose uptake or the decreased BAT uptake plays a role in the development of diabetes.

Chapter 3: Methodology and Experimental Design

3.1 Institutional Animal Care Approval

C57Bl/6J wildtype offspring mice received from McMaster University, breeders originally from the Jackson Laboratory (Bar Harbor, Maine, USA), were acclimatized for one week after arrival to Thunder Bay. They were housed in Allentown individually ventilated cages with between 2-4 mice of the same sex per cage. The cages were placed on Innovive Innorack® IVC mouse racks. Housing temperature was controlled, at 22°C ± 3°C. Each cage had a plastic enrichment dome. Mice were kept on a 12-hour light/dark cycle. Mice had unlimited access to food and water. Food was Prolab® RMH 3000.

Institutional animal care approval was received from Lakehead University Animal Care Committee and the Animal Research Ethics Board at McMaster University.

3.2 Experimental Design

3.2.1 Breeding

Male and female C57Bl/6J wildtype mice, age 7-8 weeks, were given one week to acclimate without disruption. Females were housed 5 per cage from arrival until breeding. Males were individually housed for the duration of the study. Animals had unlimited access to food and water and a 12-hour light/dark cycle was maintained. Female mice were moved to a male cage (2 females:1 male) and allowed to breed overnight. The following morning, females were removed from the male cages and individually housed. Vaginal plugs were used to determine the first day of gestation. Prior to irradiation, animals were palpated to confirm pregnancy and only pregnant mice were irradiated as described in section 3.2.2. Animals were transported to a different building for radiation treatment. Following irradiation, the mice were returned to the housing room and remained individually housed. Mothers were left uninterrupted for a minimum of one week following birth (including cage changes). Pups were weaned at 3-4

weeks of age and sex was determined. They were then housed up to 3 males or 4 female F1 pups in a cage. A maximum of two pups from a single mother was used in this study to control maternal effects.

3.2.2 Treatments

Radiation treatments were done at McMaster University. Pregnant females were exposed to ionizing radiation a single time at 1000 mGy on day 15 of gestation using ^{137}Cs gamma radiation (662 keV energy) (Taylor Radiobiology Source). The mice were transported in a temperature controlled vehicle to the Taylor Source irradiation facility. Following transportation, mice were placed under the source for 20 minutes prior to irradiation in their home cage. Sham-irradiated animals were placed under the shielded source for 20 minutes and were then moved to the control room for the duration of the irradiation. Access to food and water were restricted for the period of irradiation (sham-irradiated animals included). Radiation was delivered at a dose rate of 10 mGy/min measured using thermoluminescent dosimeters (Mirion Technologies, Irvine, California, USA) placed in the bedding of an empty animal cage with the lid on. The cages were transported back to the animal housing facility. The mice were shipped to Thunder Bay at 3 ½ months of age. Once at the Thunder Bay animal facility, the mice were left to acclimate for one week. Experiments commenced when the offspring reached 4 months $\pm$ one week of age.

3.2.3 Image Acquisition

To assess glucose uptake in interscapular brown adipose tissue (IBAT), ^{18}F-fluorodeoxyglucose (FDG) was obtained from the cyclotron (Thunder Bay Regional Health Research Institute, Thunder Bay, ON, Canada) on experiment days. A concentration of approximately 300 μCi/ml diluted with sterile saline was made following the FDG Dilution Worksheet (Appendix). A mouse was anesthetized with 1.5% isoflurane anesthetic for five minutes inside a vapour induction chamber. An intraperitoneal injection of the appropriate volume at a dose of approximately 20 μCi was given. There was a wait time of 15 minutes

between injections of each subsequent mouse to avoid scan time overlap. After 55 minutes, the mouse was anesthetized with 1.5% isoflurane for five minutes. The mouse was then placed in the imaging chamber in a prone position and inserted into the G4 PET/X-ray scanner (Sofie Biosciences, Culver City, California, USA). The imaging chamber contains a nose cone for isoflurane administration at 1.5% during the scan to maintain lack of consciousness. The base of the imaging chamber was heated to 37°C to maintain their core body temperature. A 10-minute acquisition was performed followed by an X-ray. Each mouse was subsequently imaged under the same parameters. After experimentation, mice were placed back in their original cages to recover with access to food and water.

3.2.4 Image Analysis

Glucose uptake was measured using ^{18}F-FDG radiotracer and microPET imaging. VivoQuant™(Version 1.23, Invicro, Boston) image analysis software was used to reconstruct and quantify glucose uptake in IBAT. A region of interest was selected to encompass the tissue. A draw tool was used to account for the volume of the entire tissue. From the encompassed tissue, maximum standardized uptake value (SUV_{MAX}) was calculated and reported in SUV/mm^3. SUV_{MAX} is the calculated SUV on the highest image pixel in the region.

$$SUV_{MAX} = \frac{\left(\frac{Activity\ in\ region\ (\mu Ci)}{Region\ of\ volume\ (ml)} \Big/ \frac{Injected\ dose\ (\mu Ci)}{Body\ weight\ (g)}\right)}{Volume\ (mm^3)}$$

3.2.5 Tissue Collection

One week after image acquisition, mice were anesthetized under 3% isoflurane anesthetic and the hearts removed. IBAT, livers, and hearts were immediately frozen on dry ice for future analysis. Blood was collected from the chest cavity and stored in tubes containing EDTA on ice for plasma isolation.

Within two hours, the blood was centrifuged at 3000 g for 10 minutes at 4°C. The supernatant (plasma) was collected and stored at -30°C until analysis.

3.2.6 Tissue Lysis

Frozen liver tissue was pulverized into powder using a mortar and pestle kept cold with liquid nitrogen and kept on dry ice. The powder was stored at -80°C until analysis.

For western blots, frozen liver powder was disrupted and homogenized in ice-cold lysis buffer (25mmol/L Tris pH = 7.5, 150 mmol/L NaCl, 1 mmol/L EDTA, 1% Triton-X 100) with an addition of sodium fluoride (NaF) (Sigma Life Science, St. Louis, Missouri, USA), sodium orthovanadate (Na_3VO_4) (Sigma Life Science, St. Louis, Missouri, USA) and protease inhibitor cocktail (Sigma Life Science, St. Louis, Missouri, USA). Disruption and homogenization was completed using the Qiagen TissueLyser. Samples were centrifuged at 16000 g for 10 minutes at 4°C and supernatants were collected. 1:20 dilutions were made for the protein assay and the rest of the sample stored at -80°C until further analysis could be completed.

For western blots, frozen IBAT (whole) was disrupted and homogenized in ice-cold lysis buffer (25mmol/L Tris pH = 7.5, 150 mmol/L NaCl, 1 mmol/L EDTA, 1% Triton-X 100) with an addition of sodium fluoride (NaF) (Sigma Life Science, St. Louis, Missouri, U.S.A.) and protease inhibitor cocktail (Sigma Life Science, St. Louis, Missouri, U.S.A.). Disruption and homogenization was completed using the Qiagen TissueLyser. Samples were centrifuged at 16000 g for 10 minutes at 4°C, and the intermediate layer collected. The supernatant was centrifuged a second time and the intermediate layer collected. Prepared samples were stored at -80°C until further analysis could be completed. Protein assays were completed (Pierce™ BCA Protein Assay Kit, Thermo Scientific, Rockford, Illinois, U.S.A.) to determine protein content for western blot analysis. 1:4 dilutions were made with 10% sodium dodecyl sulfate and distilled water for the protein assay.

3.2.7 Protein Assay

Prior to performing western blots, protein assays were completed to determine protein content for western blot analysis and for sample normalization. Protein assays were completed as per Pierce™ BCA Protein Assay Kit. Protein assays were performed the same day as tissue lysis to avoid the freeze-thaw cycle. Steps were followed as per Pierce™ BCA Protein Assay Kit: Samples and bovine serum albumin standards (10μl) were loaded into a Costar 96 flat bottom plate (9017) in duplicate. Once all samples were loaded, 200μl of working reagent (prepared 50:1 for reagent A:B) was added to each well containing standard or sample. The plate was mixed on the plate shaker at 200rpm for 30 seconds. After mixing, the plate was incubated at 37°C for 30 minutes. After incubation, the plate was cooled to room temperature and read at 562nm on a BioTek Power Wave XS microplate reader using Gen5 data analysis software.

3.2.8 Sample Preparation for Western Blot

After the protein assay was performed, the liver and IBAT samples were prepared for western blots. Samples were kept on ice for the duration of the preparation. A 1ml aliquot of sample reducing buffer (4X Laemmli buffer) was thawed at room temperature. Once thawed, 110μl of 100mM dithiothreitol (DTT) (Fisher Scientific, Fair Lawn, NJ, cat# BP172-25) was added to the sample reducing buffer. Using a needle, a set of 1.5ml tubes had a hole poked in each lid. Distilled water was added to each tube. 1.5μg/μl of sample was added to its corresponding 1.5ml tube. The appropriate volume of sample reducing buffer was added to each tube. The tubes were boiled at 100°C for 5 minutes. Western blot prepared samples were placed back on ice to cool. Western blot prepared samples and original samples were stored in at -80°C until western blots could be performed.

3.2.9 Western Blotting

(see Appendix for full Lees Lab Western Blot SOP)

Polyacrylamide gels were prepared at a 15% concentration for SOCS3 isolation and 10% concentration for PEPCK, UCP1, phosphorylated Akt (pAkt), Akt, phosphorylated GSK3β (pGSK3β), and GSK3β isolation. Samples prepared in section 2.3.7 were thawed on ice. 5μl of molecular ladder (BLUelf prestained protein ladder, FroggaBio, Canada, cat #PM008-500) was added to the first well. Samples were loaded alternating treatment groups. Several samples were repeated across gels as loading controls. All gels were run for 1 hour at 200 volts. Each gel was transferred to a nitrocellulose membrane. Ponceau S staining was used as a marker of equal protein loading. Ponceau S stains were quantified using ImageJ. The same four band region on each lane was selected encompassing the area where the target protein would be located based on molecular weight. Ponceau S staining was chosen instead of other loading controls because standard housekeeping proteins (e.g., GAPDH and β-actin) can be affected by different cellular process and may not accurately reflect total protein loads [143]. The blocking solution consisted of 5% powdered milk in 1XTBST (TBST: Tris Base, Molecular Biology Grade, Fisher Scientific, Fair Lawn, NJ, cat # BP152-5 + Tris Hydrochloride, Fisher Scientific, Fair Lawn, NJ, cat # BP153-500 + Tween 20, Bio Rad, Hercules, CA, USA, cat # 1706531). Immunoblotting was performed using the primary antibody: SOCS3 (Cell Signaling Technology, Danvers, MA, cat #2923), anti-PCK1 (Abcam, Cambridge, MA, cat # ab70358), UCP1 (D9D6X) Rabbit mAb (Cell Signaling Technology, 14670, Danvers, MA, USA), Phospho-Akt (Ser473)(D9E) XP® Rabbit mAb (Cell Signaling Technology, 4060, Danvers, MA, USA), Akt (pan) (C67E7) (Cell Signaling Technology, 4691, Danvers, MA, USA), Phospho-GSK-3β (Ser9) (Cell Signaling Technology, 5558, Danvers, MA, USA) or GSK-3β XP® Rabbit mAb (Cell Signaling Technology, 12456, Danvers, MA, USA). After incubation, the secondary antibody Pierce antibody goat-anti rabbit IgG (H + L) (Thermo Scientific Pierce, Rockford, IL, cat# 31460) were used for all blots. SuperSignal™ West Pico Chemiluminescent Substrate was used for SOCS3 and pAkt. For all other targets, immunoreactive complexes were detected with enhanced chemiluminescence (ChemiDoc™ XRS, Bio-Rad, Hercules, CA, USA). All blots

were quantified using ImageJ software. Loading controls were used for normalization.

3.2.10 Triglyceride Assay

Powdered liver samples were removed from the -80°C freezer and placed on dry ice. Frozen liver powder was weighed out and homogenized in ice-cold lysis buffer (5% Igepal CA-630, MP Biomedicals, Solon, OH, cat # 19859650) with addition of Protease Inhibitor Cocktail (Sigma Life Science, St. Louis, Missouri, USA). Homogenization was completed using the Qiagen Tissue Lyser. Samples were then centrifuged at 16000 g for 10 minutes at 4°C, supernatants were collected and a protein assay performed to avoid the freeze-thaw cycle of the sample. Protein assays were completed (Pierce™ BCA Protein Assay Kit, Thermo Scientific, Rockford, Illinois, USA) as per section 2.3.6 to determine protein content for normalization. Plasma samples were removed from the -30°C freezer and placed on ice to thaw.

Triglyceride assays were completed to determine hepatic and plasma triglyceride content (Triglyceride Colorimetric Assay Kit, Cayman Chemical Company, Ann Harbor, Michigan, USA). NP-40 from the kit was replaced with, a chemically indistinguishable substitute, 5% Igepal CA-630 (MP Biomedicals, Solon, OH, cat # 19859650). Samples (10μl) were loaded into a Costar 96 flat bottom plate (9017) in duplicate. Once all samples were loaded, 150μl of Enzyme Buffer was added to each well containing sample. The plate was mixed on the plate shaker at 200rpm for 30 seconds. After mixing, the plate was incubated at room temperature for 15 minutes. After incubation, the plate was read at 540nm on a BioTek Power Wave XS microplate reader (model #MQX200R) using Gen5 data analysis software.

3.3 Limitations, Basic Assumptions, and Delimitations

3.3.1 Limitations and Basic Assumptions

This study could not be performed on humans and therefore, a mouse model was adopted to study the effects of radiation. Animal models often represent physiological treatments better than cell culture models. In this study animals were used for all experiments. Based on our regular monitoring of the animals it is assumed that all mice consumed a similar amount of food and water and remained well-fed and hydrated. This strain of mouse is thought to represent healthy normal physiological conditions and assumed to be pathogen and disease free.

Other limitations are environmental factors that unknowingly affect the animals including transportation and disruption of light/dark cycles. All mice are kept in the same environment but may be exposed to stressors that may cause uncontrollable variation in results. The mice were transported to and from the irradiation facility at McMaster University 2-3 times a week starting one week prior to breeding and between gestational days 8 and 15 to minimize stress at the time of irradiation. Transport from Hamilton, Ontario to Thunder Bay, Ontario may have presented an additional stressor. While transportation acclimation was done for road transportation in the parents, the offspring were never mock transported. The offspring were flown to Thunder Bay introducing another stress event. While air travel is the main route of transport from the facility where the mice are born to a research facility, offspring that have been exposed to 1000 mGy in-utero may respond differently to the stress and have an adverse response to flying. The effects and extent of variations and how they relate to this study are unknown.

3.3.2 Delimitations

Mice are more radioresistant than humans and required a higher whole-body dose of radiation to illicit similar effects. 1000 mGy of whole-body irradiation is assumed to be similar to a low dose exposure in humans. One potential limitation of this study is the strain of mice used. C57Bl/6J mice were used

exclusively. Research regarding the potential radioresistance of C57Bl/6 mice has emerged suggesting that other strains of mice may be more sensitive to radiation. Using other strains of mice such as BALB/C, may show more significant changes in offspring related to fetal programming when the dam is exposed to the same dose of radiation. Increasing the radiation dose to produce similar effects in C57Bl/6 mice was chosen over selecting another strain so that comparisons to other models of fetal programming, which commonly use C57Bl mice, could be made. A second reason for choosing C57Bl/6J mice was for future comparison to dexamethasone studies. The final reason for choosing C57Bl/6J mice was the availability of knockout models for comparison in future studies.

Image analysis was done by the same individual to maintain consistency and limit variation as personal judgement is required when using the analysis software. Using the same individual does not allow for comparison to account for bias or skew, but for consistency one person is used for all image analysis.

3.4 Statistical Analysis

All data was presented as means ± SEM. Comparisons between treatment groups was done using two-tailed Student's *t*-tests. A resulting *p*-value of less than or equal to 0.05 was considered statistically significant.

Chapter 4. Results

4.1 Anthropometric Results

4.1.1 SLDR Exposure Did Not Alter Body Weight at 4 Months of Age

A key indicator of fetal programming is low birth weight. Birth weights were not recorded to reduce stress from handling and filial cannibalism. At 4 months of age, female offspring body weight decreased with treatment but the change was not significant (p = 0.07) (Figure 6). There was no change in body weight in the male offspring caused by maternal exposure to 1000 mGy (p =0.92) (Figure 6). It is possible that catch-up growth occurred and any differences that may have existed previously are no longer visible.

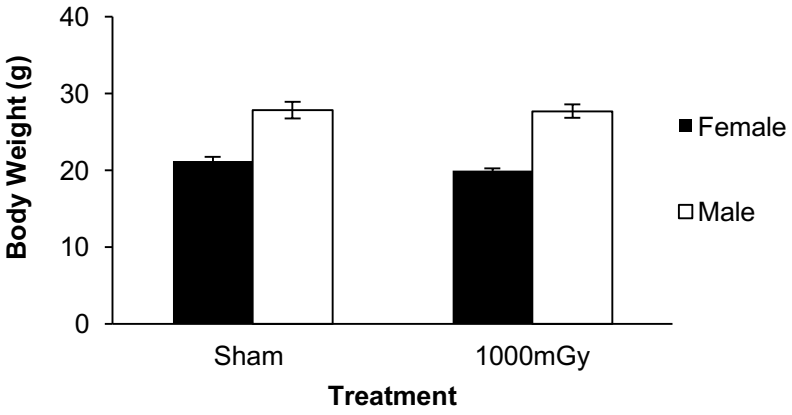

Figure 6. Body weights. There were no differences in body weight between the treatments when measured at 4 months of age. Data are presented as mean ± SEM. n = 7-10 per group.

4.1.2 SLDR Exposure Altered Female Liver Weight and Male Heart Weight

Tissue weights were collected for heart, liver, and IBAT (Table 3). Tissue weights were compared to body weight for each mouse to determine if there was any difference in tissue weight between treatment groups. Heart weight to body weight ratio decreased in the male offspring of irradiated dams (p = 0.01) (Figure 7A). Female heart weight to body weight ratio was unchanged (p = 0.81). There was no difference in the IBAT to body weight ratio in females (p = 0.36) or males (p = 0.47) with treatment (Figure 7B). Liver weight was significantly higher in

female offspring from irradiated dams ($p = 0.05$) but did not change significantly in the males ($p = 0.46$) (Figure 7C).

Table 3. Tissue weights from offspring of irradiated and sham irradiated dams.

	Male		Female	
	Sham	1000mGy	Sham	1000mGy
Body Weight (g)	27.80 ± 1.11	27.66 ± 0.87	21.14 ± 0.58	19.96 ± 0.23
Liver Weight (mg)	1262.61 ± 116.40	1170.17 ± 63.94	809.19 ± 63.33	959.42 ± 30.28*
Heart Weight (mg)	121.27 ± 7.20	103.15 ± 2.10*	87.31 ± 2.52	86.27 ± 3.39
IBAT Weight (mg)	86.51 ± 8.24	80.09 ± 4.49	50.13 ± 2.53	46.93 ± 2.24

Measurements were taken at 4 months of age. Tissue weights were taken prior to freezing. Data are presented as means ± SEM. *Significant differences ($p \leq 0.05$) between treatment groups. n = 7-10 per group.

A

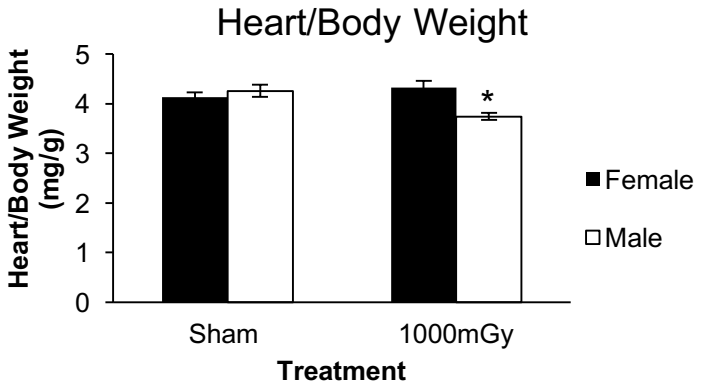

B

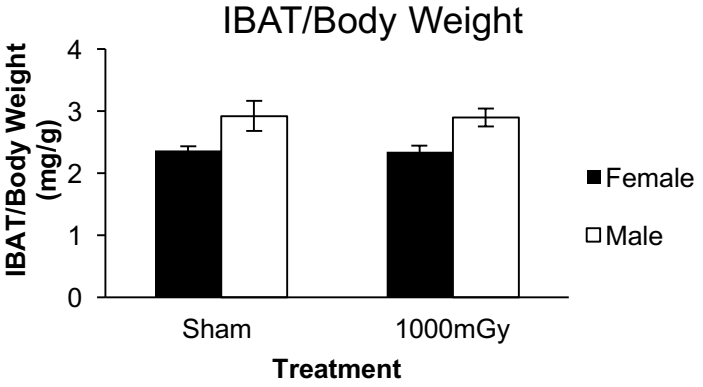

C

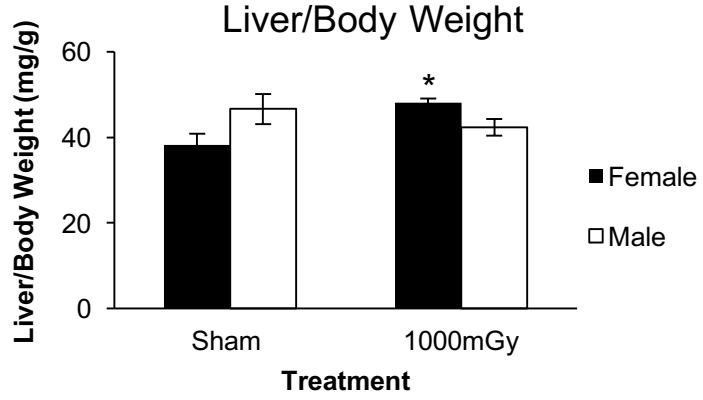

Figure 7. Tissue to body weights. Measured one week after microPET imaging. Black bars represent female tissue weight. White bars represent male tissue weight. *Significant differences ($p \leq 0.05$) between treatment groups. Data are presented as mean ± SEM. n = 7-10 per group.

4.2 Proteins Involved in Glucose Metabolism in the Liver

4.2.1 Increased Hepatic SOCS3 in Female Offspring

The female offspring of irradiated dams had significantly increased SOCS3 protein expression by 20% compared to offspring from sham irradiated dams (p = 0.03) (Figure 8A). There was a 27% difference in SOCS3 protein expression between male sham and male 1000 mGy treatment groups but it was not significant (p = 0.07) (Figure 8B). Unexpectedly, there was a trend towards the opposite effect as the females, where males from irradiated dams had lower protein expression of SOCS3.

A

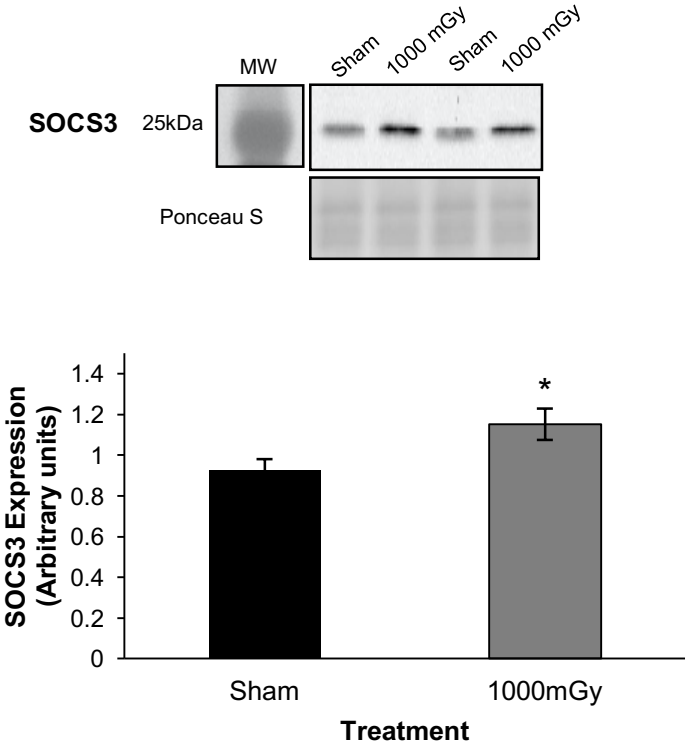

B

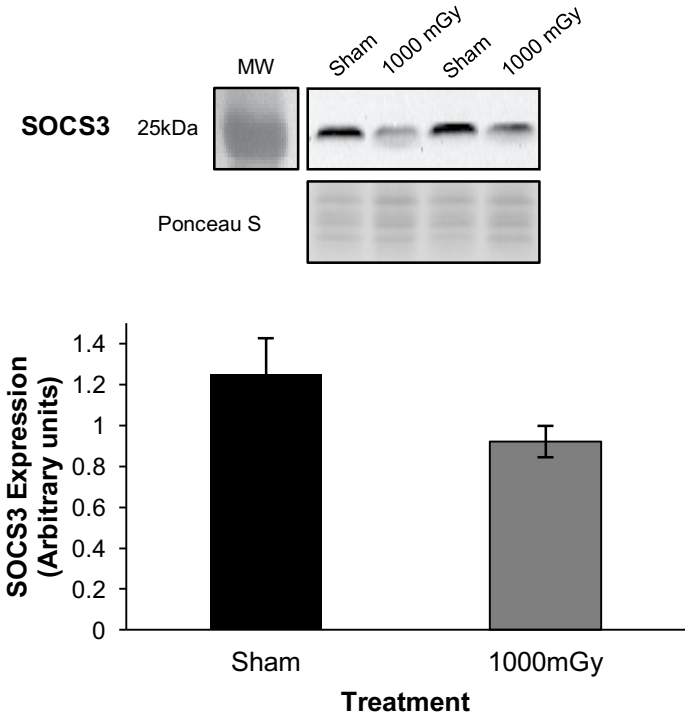

Figure 8. Liver SOCS3 protein expression from offspring of irradiated and sham irradiated dams at 4 months of age. (A) Representative western blot of SOCS3 in female mice. Black bar represents SOCS3 protein expression in the liver of sham irradiated female offspring. Grey bar represents SOCS3 protein expression in the liver of female offspring from irradiated dams. (B) Representative western blot of SOCS3 in male mice. Black bar represents SOCS3 protein expression in the liver of sham irradiated male offspring. Grey bar represents SOCS3 protein expression in the liver of male offspring from dams irradiated at 1000 mGy. Results were normalized to loading controls. Ponceau S stains are shown as markers of equal protein loading. *Significant differences ($p \leq 0.05$) between treatment groups. Data are presented as mean $\pm$ SEM. n = 7-10 per group.

4.2.2 Increased Hepatic PEPCK in Female Offspring

The female offspring of irradiated dams had significantly increased (15%) protein expression of PEPCK in the liver compared to the offspring of sham irradiated dams (p = 0.002) (Figure 9A). There was an 12% decrease in PEPCK protein expression between male sham and male 1000 mGy treatment groups but it was not significant (p = 0.06) (Figure 9B).

A

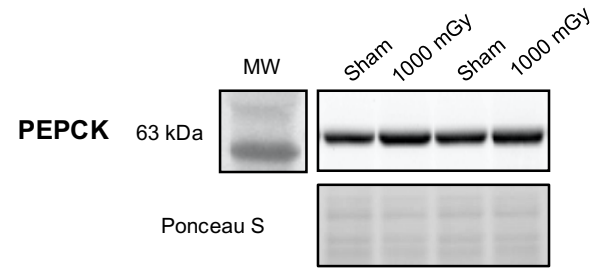

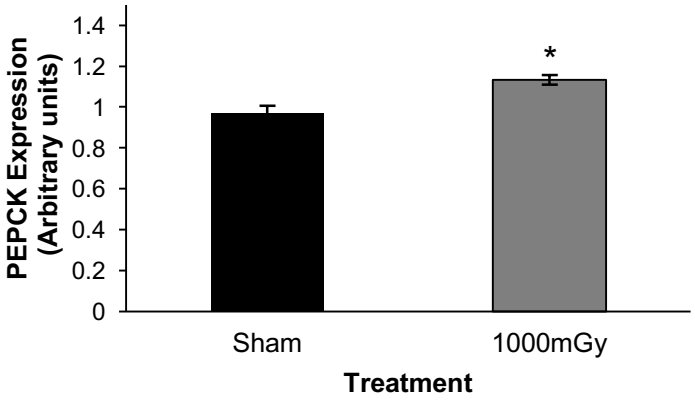

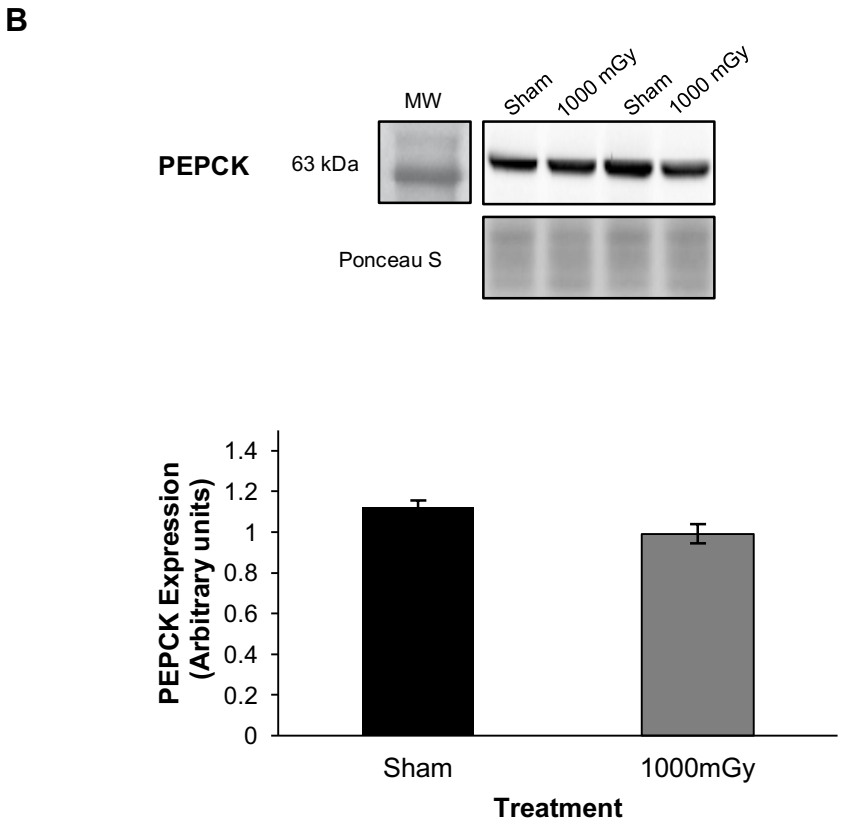

Figure 9. Liver PEPCK protein expression from offspring of irradiated and sham irradiated dams at 4 months of age. (A) Representative western blot of PEPCK in female mice. Black bar represents PEPCK protein expression in the liver of sham irradiated female offspring. Grey bar represents PEPCK protein expression in the liver of female offspring from irradiated dams. (B) Representative western blot of PEPCK in male mice. Black bar represents PEPCK protein expression in the liver of sham irradiated male offspring. Grey bar represents PEPCK protein expression in the liver of male offspring from irradiated dams. Results were normalized to loading controls. Ponceau S stains are shown as markers of equal protein loading. *Significant differences ($p \leq 0.05$) between treatment groups. Data are presented as mean ± SEM. n = 7-10 per group.

4.3 Hepatic and Plasma Triglyceride Content

A triglyceride assay was performed on liver tissue dissected from the mice at 4 months of age. No difference was observed in hepatic triglyceride content in the females based on treatment (p = 0.45) (Figure 10A). However, in the male offspring, the 1000 mGy treatment group has higher hepatic triglyceride content than the sham group (p= 0.02) (Figure 10B). Female plasma triglyceride concentration increased by 28% with treatment but the change was not significant (p = 0.08) (Figure 11A). No differences were observed from treatment in plasma triglyceride levels in the males (p = 0.67) (Figure 11B).

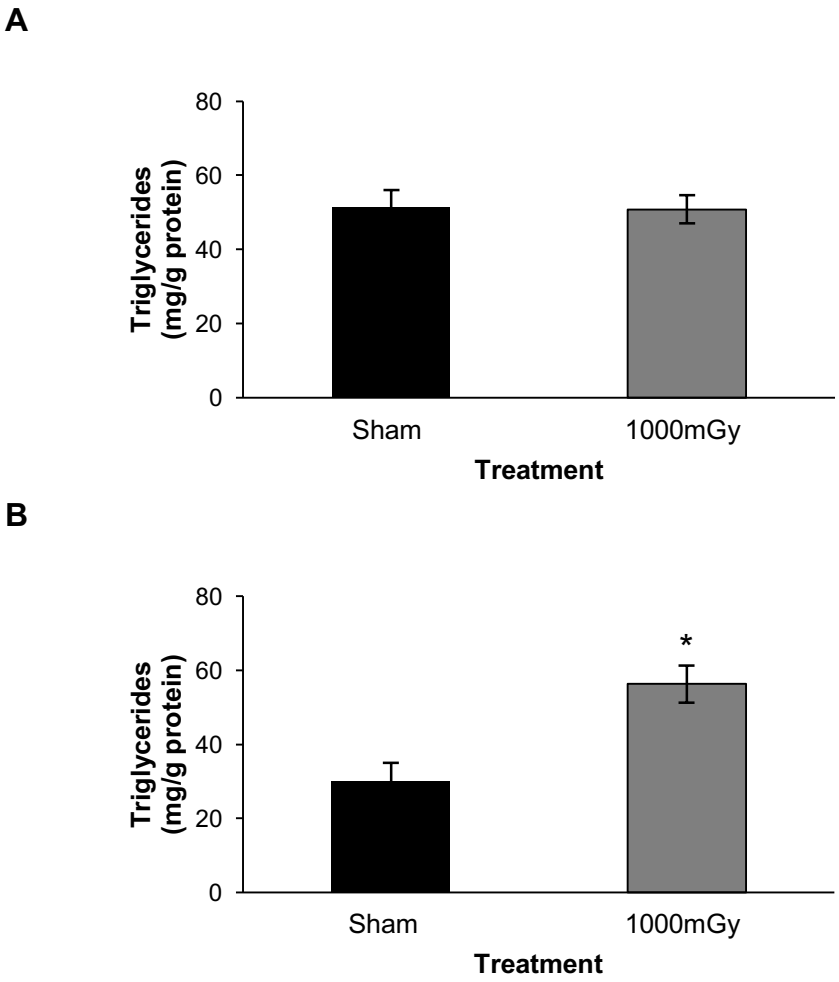

Figure 10. Triglyceride content in the liver. (A) Female hepatic triglyceride content. Black bar represents hepatic triglyceride content in female sham irradiated offspring. Grey bar represents hepatic triglyceride content in female offspring of irradiated dams. (B) Male hepatic triglyceride content. Black bar represents hepatic triglyceride content in male sham irradiated offspring. Grey bar represents hepatic triglyceride content in male offspring of irradiated dams. Triglyceride content was normalized to liver protein content. *Significant differences ($p \leq 0.05$) between treatment groups. Data are presented as mean ± SEM. n = 7-10 per group.

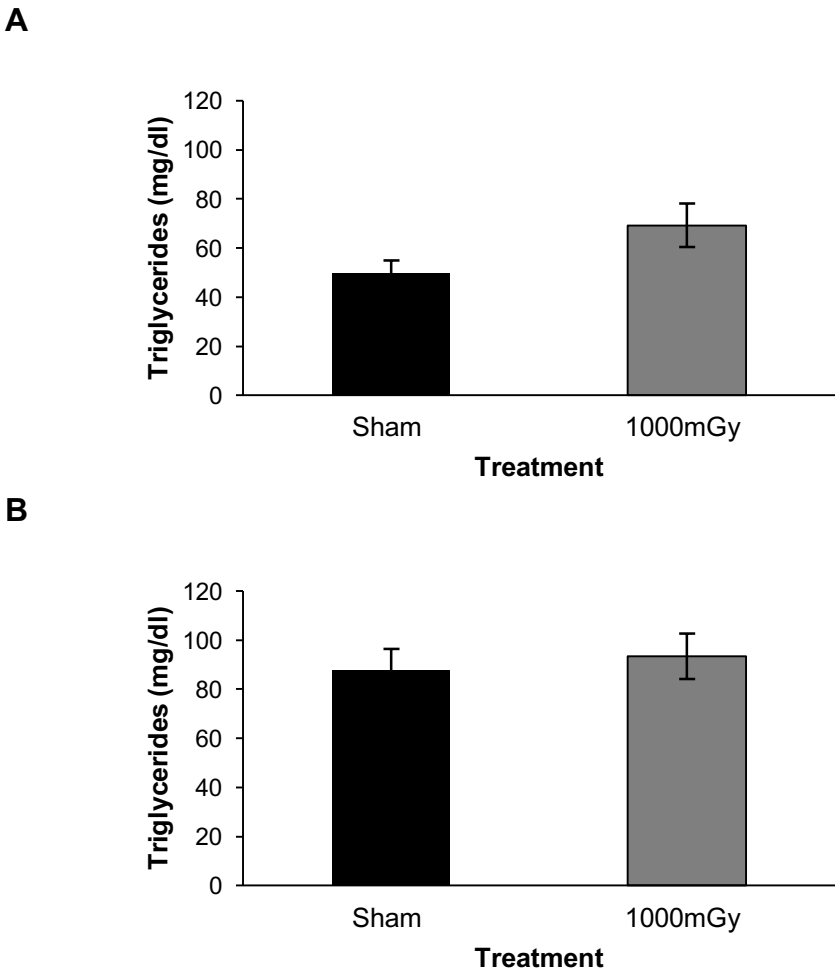

Figure 11. Plasma triglyceride concentration. (A) Female plasma triglyceride concentration. Black bar represents plasma triglyceride concentration in female sham irradiated offspring. Grey bar represents plasma triglyceride concentration in female offspring of irradiated dams. (B) Male plasma triglyceride concentration. Black bar represents plasma triglyceride concentration in male sham irradiated offspring. Grey bar represents plasma triglyceride concentration in male offspring of irradiated dams. *Significant differences ($p \leq 0.05$) between treatment groups. Data are presented as mean $\pm$ SEM. n = 7-10 per group.

4.5 Glucose Uptake Increased in Female Offspring IBAT

Tissue specific glucose uptake was measured *in vivo* with a 10-minute static PET scan with ^{18}F-FDG. Glucose uptake increased by 36% in female offspring of dams irradiated at 1000 mGy compared to female sham offspring (p = 0.003) (Figure 12). There was no significant change with treatment in the male offspring (p = 0.35). Changes in uptake are presented as SUV_{MAX}.

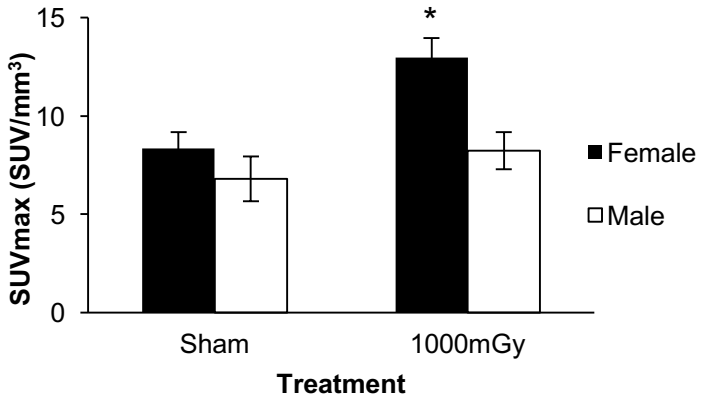

Figure 12. ^{18}F-FDG uptake. Black bars represent female IBAT ^{18}F-FDG uptake. White bars represent male IBAT ^{18}F-FDG uptake. *Significant differences ($p \leq$ 0.05) between treatment groups. Data are presented as mean ± SEM. n = 7-10 per group.

4.6 IBAT Signaling

4.6.1 No Detectable Changes in Akt Protein Expression or Phosphorylation

The phosphorylation and expression of Akt, a signaling protein associated with insulin signaling was measured in IBAT. In female offspring, treatment did not result in significant changes in phosphorylated Akt Ser473 (pAkt) (p = 0.99) or total Akt (p = 0.70) (Figure 13B). When presented as a ratio of pAkt to total Akt, there remain no difference in the females (p = 0.79) (Figure 13C). In male offspring, there are no significant changes in pAkt (p = 0.80) or total Akt (p = 0.60) (Figure 14B). Figure 14C shows the ratio of pAkt to total Akt in male offspring for the treatment groups where no significant change is observed (p = 0.67).

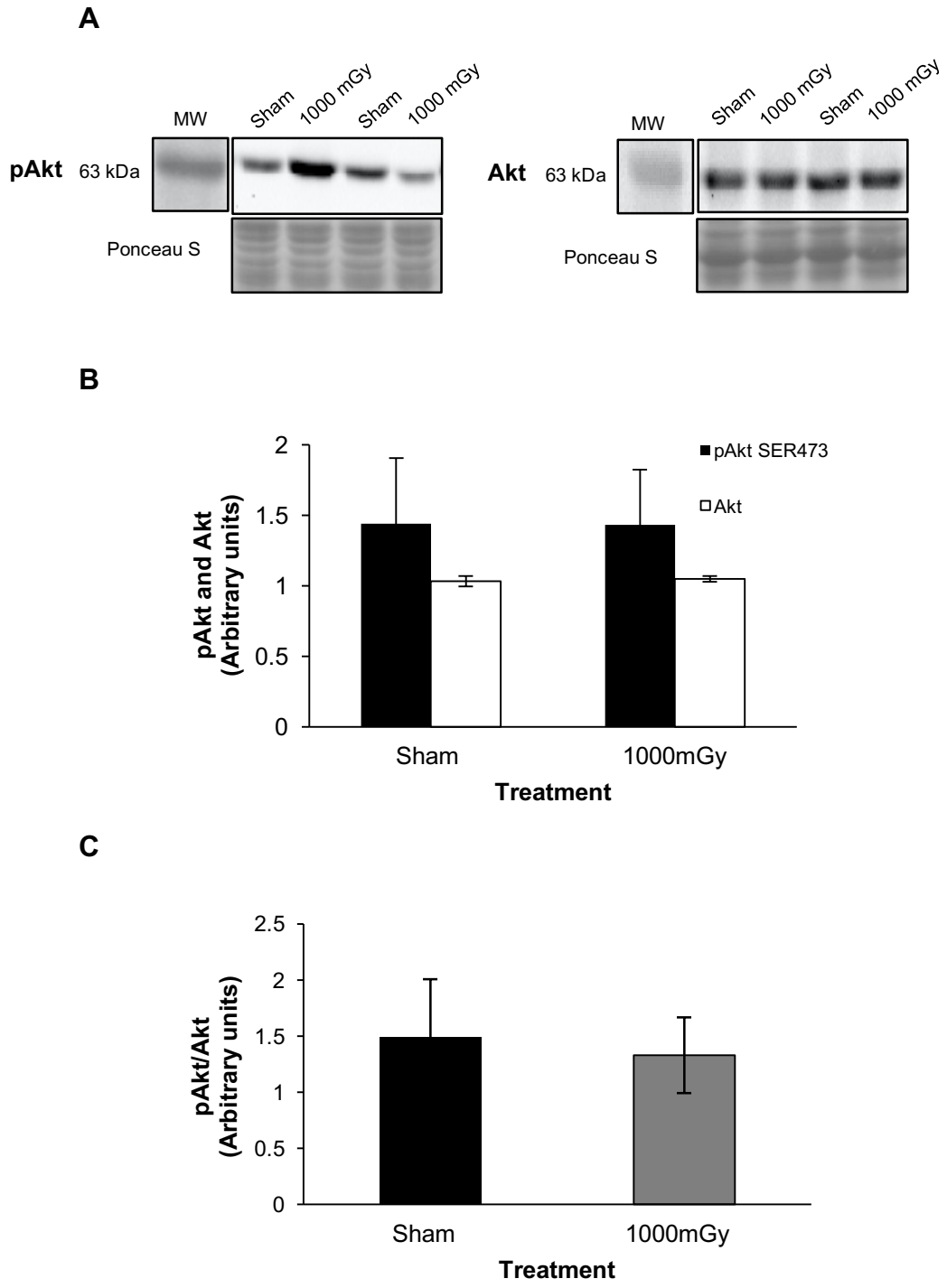

Figure 13. Female phosphorylated Akt (Ser473) (pAkt) and total Akt protein expression. (A) Representative western blots for pAkt and total Akt in IBAT from female offspring of sham and irradiated dams. Ponceau S stains are shown as markers of equal protein loading. (B) Black bars represent pAkt protein expression. White bars represent total Akt protein expression. (C) Black bar

represents ratio of pAkt to total Akt protein expression in female offspring of sham irradiated dams. Grey bar represents ratio of pAkt to total Akt protein expression in female offspring of dams irradiated at 1000 mGy. Results were normalized to loading controls. Data are presented as mean ± SEM. n = 7-10.

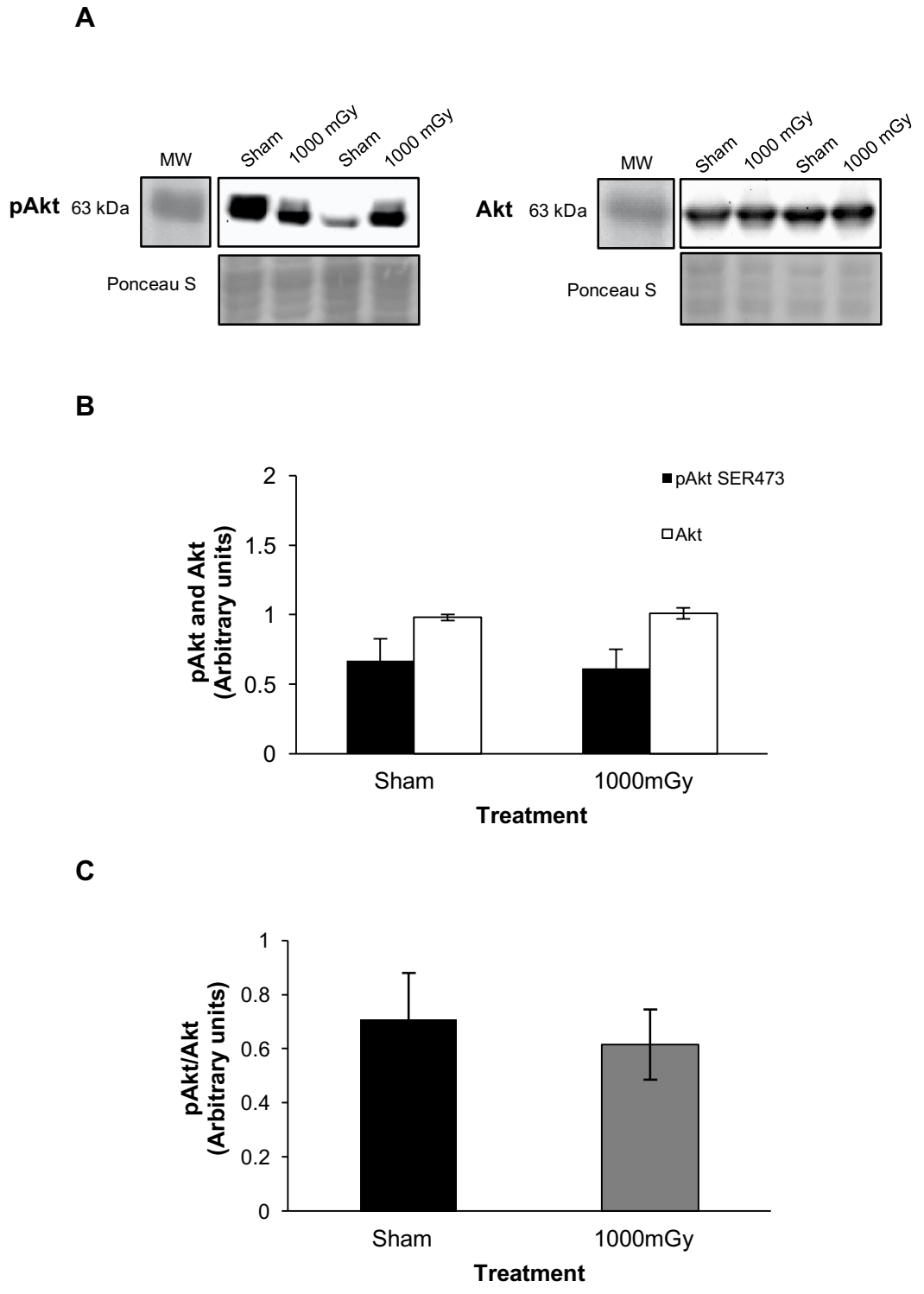

Figure 14. Male phosphorylated Akt Ser473 (pAkt) and total Akt protein expression. (A) Representative western blots for pAkt and total Akt in IBAT from male offspring of sham and irradiated dams. Ponceau S stains are shown as markers of equal protein loading. (B) Black bars represent pAkt protein

expression. White bars represent total Akt protein expression. (C) Black bar represents ratio of pAkt to total Akt protein expression in male offspring of sham irradiated dams. Grey bar represents ratio of pAkt to total Akt protein expression in male offspring of dams irradiated at 1000 mGy. Results were normalized to loading controls. Data are presented as mean ± SEM. n = 7-10.

4.6.2 Non-significant Increase in Phosphorylated GSK3β

The phosphorylation and expression of GSK3β, a signaling protein associated with β-adrenergic signaling was measured in IBAT. There was no difference in total GSK3β protein expression in the female offspring with treatment (p = 0.43) and phosphorylated GSK3β Ser9 (pGSK3β) protein expression increased by 41% but the change was not significant because of the variability between samples (p = 0.27) (Figure 15B). There was no change observed in the ratio of pGSK3β to total GSK3β in females with treatment when compared to sham irradiated (p = 0.82) (Figure 15C). In the males, there were non-significant increases of 14% in total GSK3β protein expression (p = 0.31) and 36% in pGSK3β protein expression (p = 0.22) (Figure 16B). The ratio of pGSK3β to total GSK3β for males increased by 31% but was not significant (p = 0.36) (Figure16C).

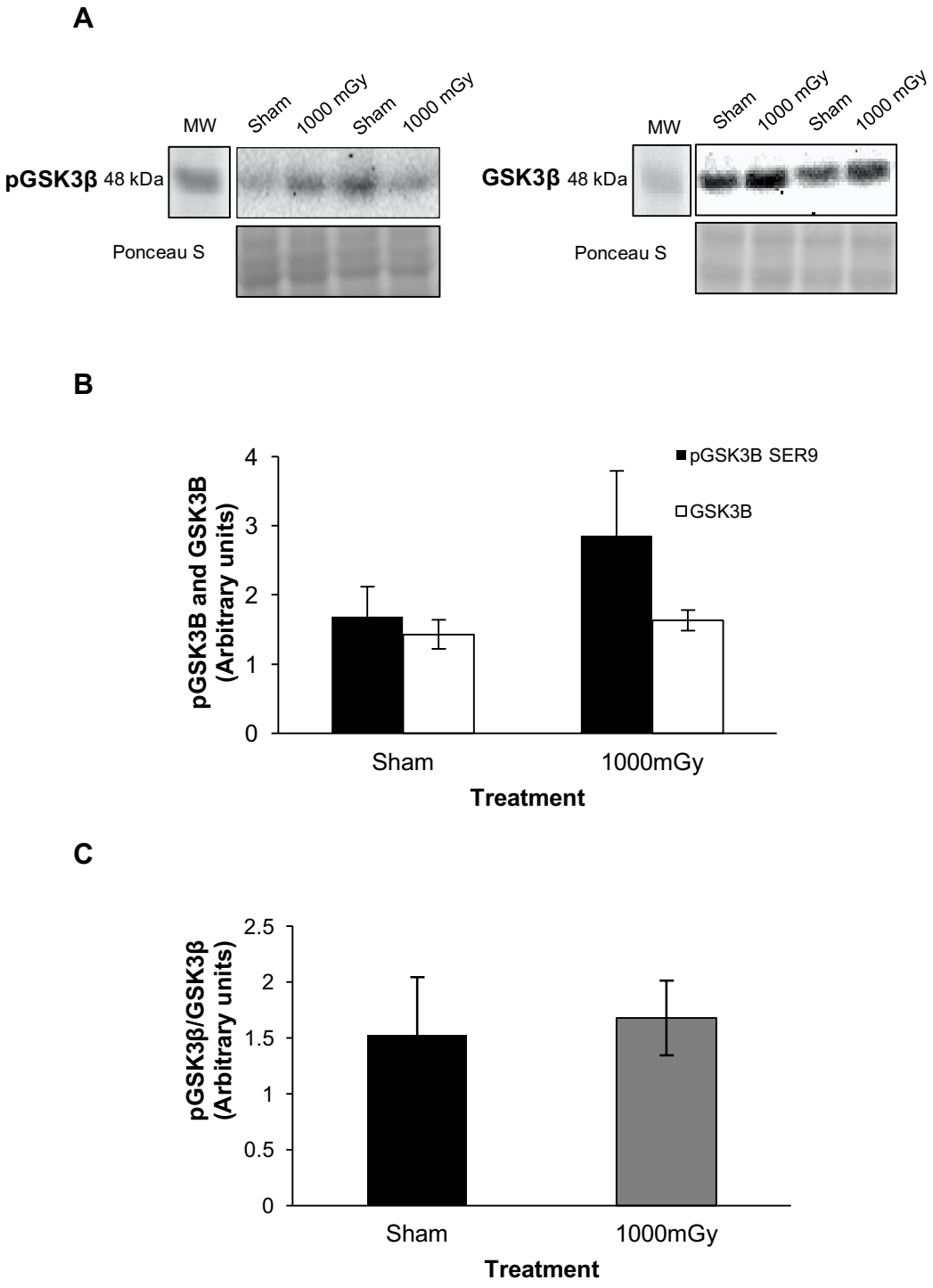

Figure 15. Phosphorylated GSK3β Ser9 (pGSK3β) and total GSK3β protein expression. (A) Representative western blots for pGSK3β and total GSK3β in IBAT from female offspring of sham and irradiated dams. Ponceau S stains are shown as markers of equal protein loading. (B) Black bars represent pGSK3β

protein expression. White bars represent total GSK3β protein expression. (C) Black bar represents ratio of pGSK3β to total GSK3β protein expression in female offspring of sham irradiated dams. Grey bar represents ratio of ratio of pGSK3β to total GSK3β in female offspring of dams irradiated at 1000 mGy. Results were normalized to loading controls. Data are presented as mean ± SEM. n = 7-10.

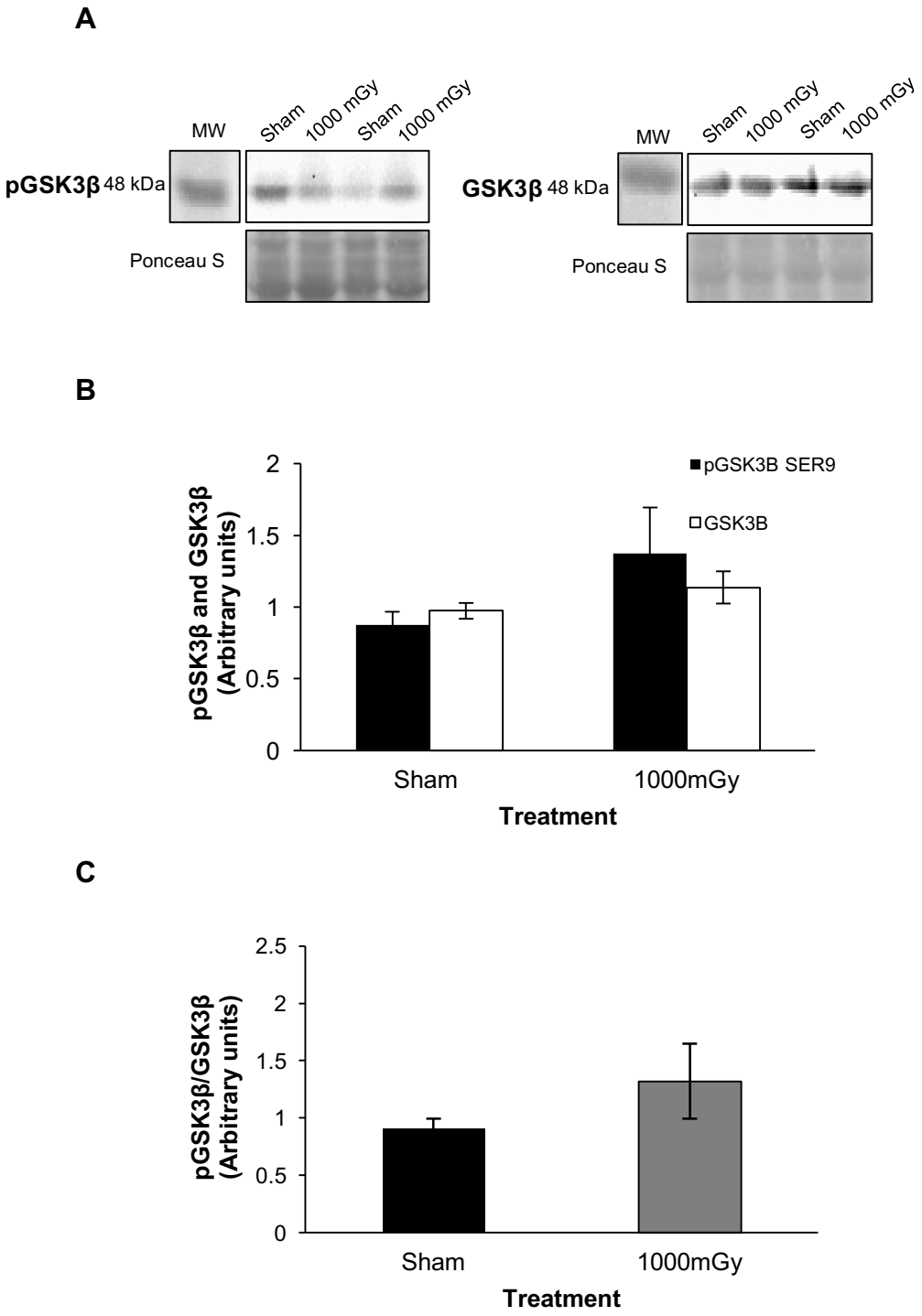

Figure 16. Phosphorylated GSK3β Ser9 (pGSK3β) and total GSK3β protein expression. (A) Representative western blots for pGSK3β and total GSK3β in IBAT from male offspring of sham and irradiated dams. Ponceau S stains are shown as markers of equal protein loading. (B) Black bars represent pGSK3β

protein expression. White bars represent total GSK3β protein expression. (C) Black bar represents ratio of pGSK3β to total GSK3β protein expression in male offspring of sham irradiated dams. Grey bar represents ratio of ratio of pGSK3β to total GSK3β in male offspring of dams irradiated at 1000 mGy. Results were normalized to loading controls. Data are presented as mean ± SEM. n = 7-10.

4.6.3 UCP1 Protein Expression Did Not Significantly Change

The presence of UCP1 can clarify that the tissue being tested is brown adipose tissue as opposed to white adipose tissue. It is also used as a marker of thermogenesis and is activated by β-adrenergic signaling. UCP1 protein expression changed between treatments by 9% in the females but was not significant (p = 0.07) (Figure 17A). There was no significant change in males (p = 0.69) (Figure 17B).

A

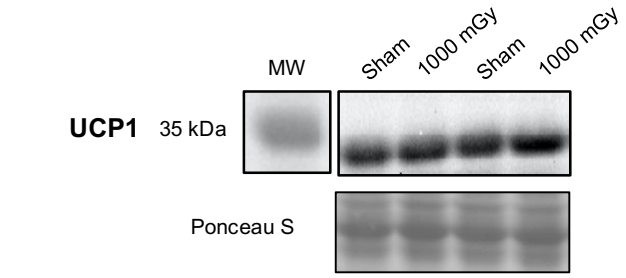

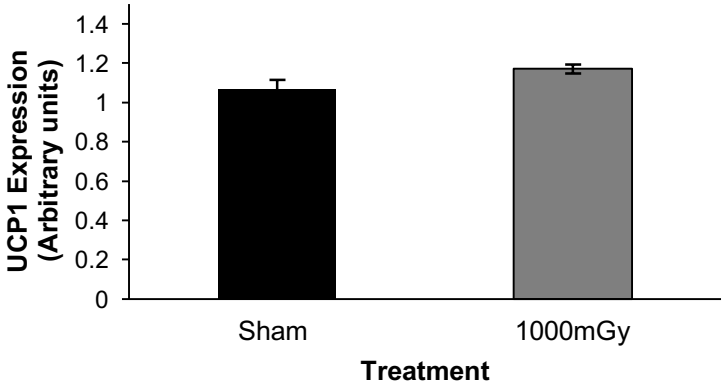

B

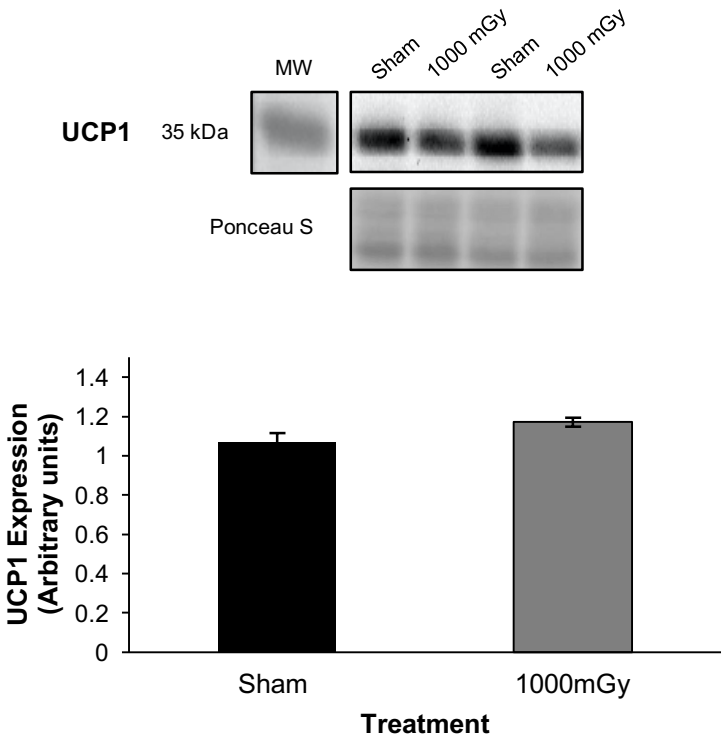

Figure 17. UCP1 protein expression from offspring of irradiated and sham irradiated dams at 4 months of age. (A) Representative western blot of UCP1 in IBAT of female mice. Black bar represents UCP1 protein expression in the liver of sham irradiated female offspring. Grey bar represents UCP1 protein expression in female offspring from irradiated dams. (B) Representative western blot of UCP1 in IBAT of male mice. Black bar represents UCP1 protein expression of sham irradiated male offspring. Grey bar represents UCP1 protein expression in male offspring from irradiated dams. Results were normalized to loading controls. Ponceau S stains are shown as markers of equal protein loading. *Significant differences ($p \leq 0.05$) between treatment groups. Data are presented as mean ± SEM. n = 7-10 per group.

Chapter 5. Discussion

This study examined the effects of sub-lethal radiation on glucose metabolism of mice. The assumption is that radiation is dangerous and concerns arise in the workplace and among the general public. While radiation protection regulations and standards are in place to prevent repeated and prolonged exposure, there are concerns about low dose exposures in humans. Even less is known about the effects of LDR when exposed in-utero. Radiation exposure during pregnancy presents a stress event that has the potential to permanently alter fetal metabolic processes. The effects may not be observable at birth or in early life but adult disease may arise at a younger age than expected. To investigate alterations in physiology and metabolism, a mouse model using sub-lethal dose radiation was used. The outcomes can be helpful in estimating the effects of LDR on fetal programming in humans. Based on the results from liver protein expression of targets associated with insulin resistance and alterations in IBAT glucose uptake, fetal programming can be caused by a sub-lethal dose of radiation in mice.

5.1 Birth Weight and Catch-up Growth

While it was expected that offspring born to irradiated dams would exhibit low birth weights (LBW) similar to other models of fetal programming, birth weights were not recorded to minimize handling stress and cannibalism. LBW is associated with long-term metabolic consequences in humans including impaired glucose tolerance, type 2 diabetes, hypertension and cardiovascular disease [40], [144]. LBW could have provided insight to the early effects of radiation on the fetus. For example, if the level of stress hormones crossing the placenta increased affecting the fetal HPA axis or if the stress from radiation altered the metabolism of the mother limiting the necessary nutrients from reaching the fetus. Although no change was observed in body weight (Figure 6), this may be the result of postnatal catch-up growth. Catch-up growth is a type of compensation where growth is

accelerated until a normal height or weight for age is reached [145]. It is common after a period of slow or impaired growth like IUGR from maternal low protein diet [146]. Catch-up growth has been shown to be important in the programming of metabolic disease risk [147]–[149]. While we have no evidence that offspring were born at LBW or catch-up occurred, it would explain the alterations observed in liver glucose metabolism.

5.2 Tissue Weight and Disease Development

Previously, decreased heart weight has been observed in a model of fetal programming from low protein diets using rats but there were no differences in the heart weight to body weight ratio [150]. The decrease observed between the heart to body weight ratio in male mice from the present study (Figure 7A) could be the result of a species difference between rats and mice or a sex difference that wasn't noticed in the previously mentioned study because the measures for the sexes were combined [151]. Increased liver weight, as seen in the female offspring of irradiated dams (Figure 7C), could indicate triglyceride or lipid build up in the liver called hepatic steatosis which is an indicator of pathophysiology like non-alcoholic fatty liver disease (NAFLD) [151]. NAFLD is likely to develop as a result of obesity or high fat diet and is linked to other metabolic alterations like insulin resistance [151], [152]. The chow used was standard and not high in fat so it was unexpected to observe increased liver weight. However, the mice had unlimited access to food and water and didn't record food consumption. There were no visibly obese mice that would lead us to believe that overfeeding would be responsible for increased liver weight in the absence of obesity. Unexpectedly, the male offspring of irradiated dams had increased hepatic triglycerides and the females did not (Figure 10). Increased hepatic triglycerides are usually seen in advanced disease like NAFLD, but this was not a model of a diseased state. Further studies could be done to look at gene expression of genes involved in lipid metabolism in sham mice compared to mice irradiated in-utero at 1000 mGy to look for differences between male and female offspring.

Radiation is known to damage the liver and can induce liver disease and cirrhosis but here there is no evidence of direct liver damage to the fetus when the mother is exposed to whole-body radiation therefore, fetal programming is likely responsible for the increased liver weight in females and increased hepatic triglyceride content in the male offspring.

5.3 Metabolic Alterations in the Liver

The increased liver weight in female offspring led us to continue to examine the liver for signs of metabolic alterations. Targets of insulin resistance were measured in both sexes using protein expression from western blots. First was SOCS3, a known modulator of insulin resistance in the liver [153]. SOCS3 is a protein induced by proinflammatory cytokines that directly inhibits IRS1/IRS2 by binding to specific sites, inhibiting phosphorylation and targeting the receptor substrates for degradation (Figure 18) [154]. In turn, this causes decreased activity in downstream components of the insulin signaling pathway. Therefore, SOCS3 is important in mediating insulin stimulated glucose uptake. Insulin resistance is a common consequence of exposure to stress, where stress results in the activation of proinflammatory cytokines that will upregulate SOCS3 [155]. In models of insulin resistance, SOCS3 protein expression is elevated in the liver [154], [156]. From our results, female SOCS3 expression increased in offspring of dams that were exposed to 1000 mGy of radiation (Figure 8A) suggesting the presence of insulin resistance.

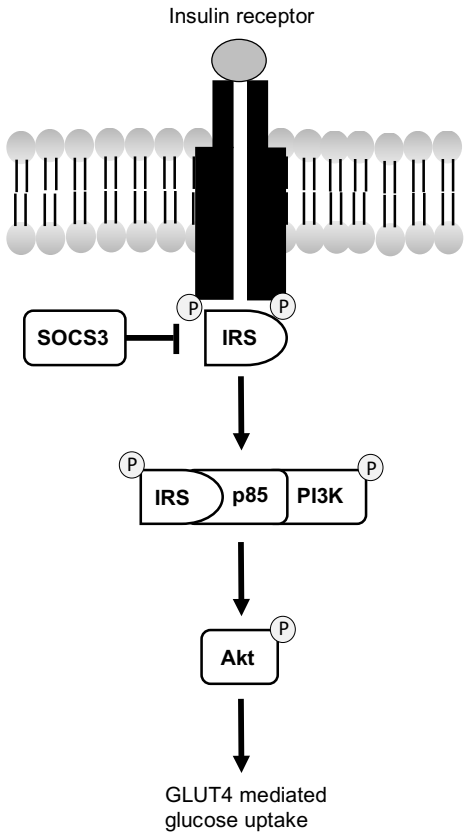

Figure 18. SOCS3 signaling. Increased SOCS3 negatively regulates insulin signaling by inhibiting insulin receptor substrate (IRS-1/IRS-2) phosphorylation and marking them as targets for degradation. This decreases activity downstream of the receptor substrates and reduces GLUT4 mediated glucose uptake into skeletal muscle. Less is known about the mechanism of SOCS3 in the liver but it is known to act on IRS1/IRS2 mediating glucose uptake into the liver. Adapted from Sarvas et al. 2013 [153].

Alone, SOCS3 is not enough to indicate insulin resistance. PEPCK was used as a second indicator of insulin resistance in the liver. PEPCK is a rate-limiting enzyme that catalyzes the first step in gluconeogenesis, the conversion of oxaloacetate to phosphoenolpyruvate, and links glucose metabolism to the citric acid cycle (Figure 19) [157]. In the liver, insulin signaling regulates gluconeogenesis by inhibiting key enzymes like PEPCK resulting in reduced hepatic glucose output. PEPCK is important in maintaining normal blood

glucose levels [158]. The activity of PEPCK is controlled by the rate of transcription of its gene by insulin, glucocorticoids and cAMP levels [159]. Overexpression of PEPCK leads to insulin resistance in the liver [160], [161]. The results of this study show increased PEPCK protein expression in females that were exposed to radiation in-utero (Figure 9A) which suggests insulin resistance. PEPCK increase also suggests gluconeogenesis would be increased in female offspring. With both targets of insulin sensitivity demonstrating increased expression, it can be concluded that female offspring of dams whole-body irradiated with 1000 mGy are more likely to be insulin resistant than the sham irradiated group.

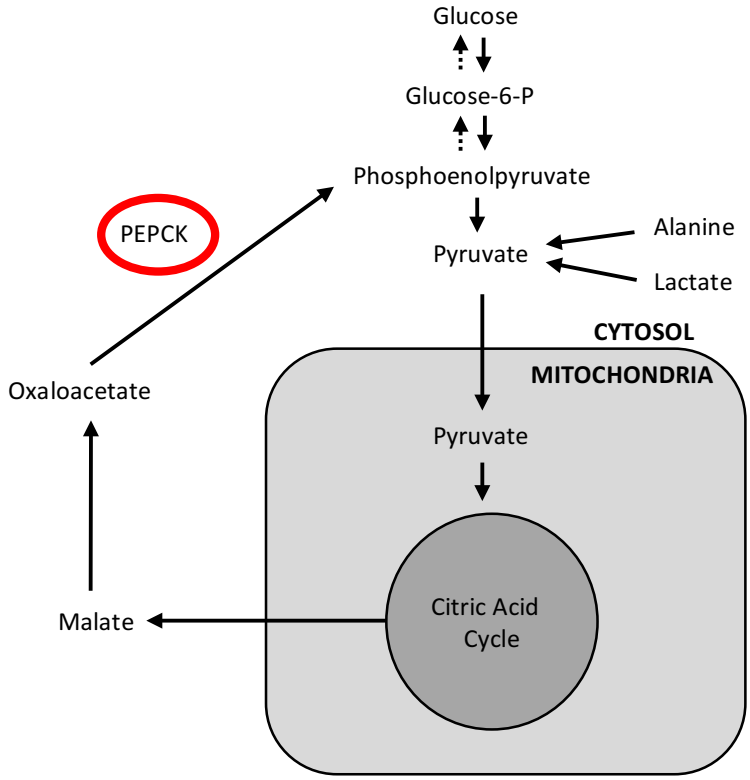

Figure 19. PEPCK in hepatic gluconeogenesis. PEPCK is an enzyme that facilitates the conversion of oxaloacetate to phosphoenolpyruvate and links glucose metabolism to the citric acid cycle. PEPCK promotes the storage of glucose as glycogen to maintain normal blood glucose levels. Adapted from Yang et al. 2009 [157].

5.4 IBAT Glucose Uptake and Signaling

Tissue specific glucose uptake was measured in IBAT with PET using ^{18}F-FDG. We report here that female offspring of irradiated dams have increased ^{18}F-FDG uptake in IBAT (Figure 12). This suggests they have hyperactive IBAT that uses more glucose and has increased energy expenditure compared to sham irradiated offspring. Since only activated BAT can be visualized, accumulation of ^{18}F-FDG indicates a high rate of glucose metabolism in the tissue. While there was no significant change in the weight of the tissue, IBAT ^{18}F-FDG uptake may have increased to compensate for whole-body glucose intolerance. Compensation like this was observed in a study by Dumortier et al. 2017, in a fetal programming model of maternal low protein diet, where insulin secretion was impaired yet mice were able to maintain normal blood glucose levels and normal insulin sensitivity [26]. They observed increased energy expenditure by indirect calorimetry and hypothesized that increased IBAT uptake acts as a protection mechanism from changes in energy homeostasis and can protect against high-fat diet induced obesity. The protective effect was maintained in mice at 10 months of age but not at 18 months. With age, BAT activity declined and the mice were more susceptible to high-fat diet induced obesity and developed insulin resistance. This is an example of how age will affect the results of fetal programming studies and is an important factor in choosing a model for experiments. It is a possibility that if the mice from our study were tested at a later age, for example at 12 months, signs of insulin resistance in the liver would be increased and IBAT activity would deteriorate in comparison to what is seen at 4 months of age.

To correlate with the increase in ^{18}F-FDG uptake in females, it was hypothesized that plasma triglyceride concentration would decrease in the offspring from the treatment group. Decreased plasma triglycerides would indicate that BAT has increased activity and is using triglycerides for energy [162]. Unexpectedly, this was not the case. The opposite trend was observed where an increase in plasma triglycerides was seen in the females (p = 0.08) (Figure 11A). Increased levels of plasma triglycerides are an indicator of leptin

resistance [163]. Leptin is a hormone released by adipose tissue signaling starvation or hunger to the brain [164]. Leptin resistance means leptin levels in the body are high but the body itself does not require food and can lead to weight gain and obesity. Leptin levels were not measured in this study but could be a focus in the future to help explain the increased plasma triglycerides. Elevated plasma triglycerides are also a symptom of metabolic syndrome [40]. The compensation period may be ending in this cohort of mice and evidence of metabolic disease is becoming more obvious without the decrease in IBAT activity. The disappearance of increased IBAT activity as compensation for impaired glucose metabolism would not be expected until later in life.

Phosphorylation of both Akt and GSK3β would have indicated that glucose uptake in IBAT is stimulated by insulin signaling [165] (Figure 4). However, there was no change in total Akt expression or more importantly phosphorylated Akt (Figure 13 & 14). The increase in phosphorylated GSK3β alone suggests the glucose uptake in female offspring IBAT is stimulated by β-adrenergic signaling (Figure 15). The phosphorylated form of these targets is more important because they will continue to move downstream in their pathways.

The difficulty of IBAT tissue preparation made it hard to choose a target for β-adrenergic signaling. While there may exist a better target than GSK3β, the size of IBAT deterred us from cutting the tissue and the difficulty of breaking down the tissue led us to use only one method of preparation. This limited the type of tests we could run. Additionally, finding a different target for β-adrenergic signaling that doesn't cross talk between pathways has yet to be established. In the future, a different tissue preparation method could be used to perform an enzyme-linked immunosorbent assay to measure cAMP as a target for β-adrenergic signaling in IBAT.

To corroborate the results of GSK3β expression, we looked at UCP1 expression in IBAT. The presence of UCP1 in females and males from both treatment groups confirm that it is indeed BAT that we are testing since white adipose tissue does not contain this protein [108]. Additionally, the presence of UCP1 implies that the tissue is capable of thermogenesis. As mentioned

previously, UCP1 is activated through the β-adrenergic pathway (Figure 3). The increase in UCP1 expression in female offspring of irradiated dams (Figure17), while not significant (p = 0.07), in combination with the increase seen in phosphorylated GSK3β show a trend toward the β-adrenergic pathway being responsible for the increase in female IBAT uptake. This is not surprising since β-adrenergic signaling is responsible for majority of the activity in BAT [31]–[34].

5.5 Factors that Affect Fetal Programming

The first factor that can affect the results of a fetal programming study is timing. The time point chosen for the stress event during pregnancy affects the severity and visibility of the effects. Day 15 of gestation was chosen for this model because previous fetal programming studies have shown that exposure during the third trimester, usually gestational days 15 to19, induce observable changes in offspring [22], [23], [166], [167]. Only a one-time dose was given at day 15 of gestation. It's a possibility that spreading the radiation treatments out over 3-4 days and having an accumulation dose of 1000 mGy rather than a one-time whole-body irradiation would alter the outcome. The first exposure, because it would be significantly less than 1000 mGy, may act like a primer to each subsequent dose reducing the negative effects on the fetus.

The time point chosen to test for alterations is also important. Studies have shown that changes in the offspring from fetal programming appear at 3 months of age and persist to 18 months of age with increasing severity of disease and metabolic dysfunction with age [26], [168], [169]. The metabolic alterations observed in this study are not a result of aging because the mice are only 4 months old and considered young adults.

The second factor that affects the measures is if the animals are in fed state or fasted. In fed state, or postprandial, insulin has been released stimulating glycogen synthesis and suppressing gluconeogenesis [170]. Fasting would

reduce variability but it would also stimulate β-adrenergic signaling and increase fatty acid release [171]. Fasting the animals prior to dissection and blood collection would have reduced variability but could not represent a normal metabolic status of the mice. Because the animals were in fed state for our study, it is not surprising that there is a huge amount of variation in the expression of phosphorylated Akt and GSK. Fed state would also explain why the plasma triglyceride concentrations vary significantly. However, fed state demonstrates glucose uptake and metabolism in a normal state which is important for IBAT ^{18}F-FDG uptake measures. Also, it prevents the additional stress from fasting.

It was not a surprise that sex differences were evident throughout this study. As expected the average body weights and tissue weights were higher for males than for females. However, sexual dimorphism continues to appear throughout the targets measured in this study. When measuring insulin resistance, female protein expression of SOCS3 and PEPCK increased with treatment whereas, the males showed the opposite trend and protein expression decreased (Figures 8 & 9). Plasma triglyceride concentration was higher in the males and male hepatic triglyceride content increased with treatment whereas females showed no difference (Figures 10 & 11). The significant differences between males and females seen in the results of this study are not surprising based on previous fetal programming literature that have found sex differences in cardiovascular and metabolic function [172], [173]. The changes seen may be a result of differences in hormone concentrations between males and females. All sex hormones are present in both male and females. In females, the human estrous cycle is 28 days and rodents have a 4-day estrous cycle. Depending on the time point in the estrous cycle, protein expression in the liver and brown adipose may vary because of the changes in hormone levels. Figure 20 shows fluctuations in estrogen, progesterone, luteinizing hormone (LH), and follicle-stimulating hormone (FSH) during one cycle in humans and rodents. These four hormones peak at different times during the cycle. Shen and Shi 2015, review the different sex hormones and their roles in glucose and lipid homeostasis in the liver [174]. Fernández-Pérez et al. 2013, discuss responses of the liver to

estrogen and growth hormone that result in sexual dimorphism [175]. The effects of estrogen on the liver can be direct or indirect through growth hormone (GH) function or by influencing pituitary GH secretion. Various hepatic genes are up- or down-regulated by different patterns in GH and sex-steroids and can affect glucose and lipid metabolism [175]. There are still uncertainties about the roles of sex hormones and their underlying, possibly protective, mechanisms in fetal programming.

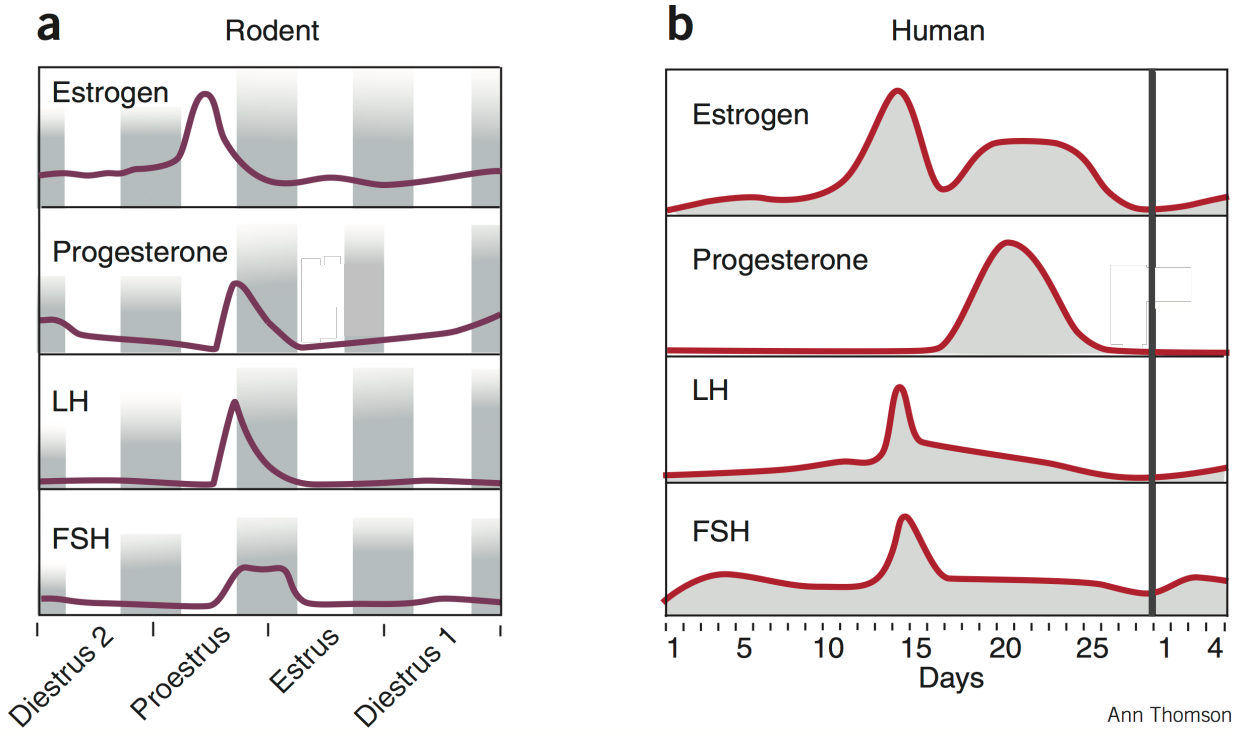

Figure 20. Changes in sex hormones during the human and rodent estrous cycles. Fluctuations in hormones levels of estrogen, progesterone, luteinizing hormone (LH), and follicle-stimulating hormone (FSH) occur during the (A) 4-day rodent estrous cycle and (B) 28-day human cycle. The grey bars indicate night (6pm to 6am). Taken from Staley and Scarfman 2005 [176], adapted from Neill and Knobil [177].

Chapter 6. Conclusion

An area of concern is the potential for long term effects on the offspring from prenatal radiation exposure. Sub-lethal doses of radiation in mice are assumed to be equivalent to low dose radiation exposure in humans. The effects on the offspring observed in this study from 1000 mGy whole-body irradiations on the dams, suggest that a one-time sub-lethal dose causes physiological changes in metabolic activity in the female liver based on increases in protein expression of targets of insulin resistance, SOCS3 and PEPCK. BAT uptake was significantly increased in the female offspring of irradiated dams and it is likely caused by β-adrenergic signaling and not insulin signaling from the non-significant increase in UCP1 and phosphorylated GSK3β protein expression. Changes are significant at 4 months of age but may be exacerbated over time. This research supplements the need for better characterization of the effects of prenatal sub-lethal dose radiation exposure in mice and low dose radiation in humans to assess risk during pregnancy.

Chapter 7. Future Directions

The present study opens the floor for several additional studies to look at alterations in glucose metabolism from fetal programming caused by radiation. It is a possibility that the changes in metabolism observed in this study may have been exacerbated if the animals were older. Experimenting with animals at 6, 12, or 18 months of age would provide a better understanding of radiation fetal programming models. Examining the effects of a dose response of radiation on fetal programming would aid in understanding the threshold of metabolic changes in mice. Our lab, along with researchers at McMaster University are currently working on a dose-response study using Sham, 50 mGy, 300 mGy and 1000 mGy radiation doses in C57Bl/6J mice. Additionally, an attempt should be made to find a new western blot target for β-adrenergic signaling in IBAT that does not crosstalk between pathways.

Chapter 8. Bibliography

[1] D. J. P. Barker, “The origins of the developmental origins theory,” *J. Intern. Med.*, vol. 261, no. 5, pp. 412–417, May 2007.

[2] L. Rui, “Energy metabolism in the liver,” *Compr. Physiol.*, vol. 4, no. 1, pp. 177–197, Jan. 2014.

[3] A. L. Birkenfeld and G. I. Shulman, “Nonalcoholic fatty liver disease, hepatic insulin resistance, and type 2 diabetes,” *Hepatol. Baltim. Md*, vol. 59, no. 2, pp. 713–723, Feb. 2014.

[4] A. P. L. Jensen-Urstad and C. F. Semenkovich, “Fatty acid synthase and liver triglyceride metabolism: housekeeper or messenger?,” *Biochim. Biophys. Acta*, vol. 1821, no. 5, pp. 747–753, May 2012.

[5] N. D. Riediger and I. Clara, “Prevalence of metabolic syndrome in the Canadian adult population,” *CMAJ Can. Med. Assoc. J. J. Assoc. Medicale Can.*, vol. 183, no. 15, pp. E1127-1134, Oct. 2011.

[6] C. A. Maloney, A. K. Gosby, J. L. Phuyal, G. S. Denyer, J. M. Bryson, and I. D. Caterson, “Site-specific changes in the expression of fat-partitioning genes in weanling rats exposed to a low-protein diet in utero,” *Obes. Res.*, vol. 11, no. 3, pp. 461–468, Mar. 2003.

[7] A. Fedorenko, P. V. Lishko, and Y. Kirichok, “Mechanism of fatty-acid-dependent UCP1 uncoupling in brown fat mitochondria,” *Cell*, vol. 151, no. 2, pp. 400–413, Oct. 2012.

[8] J. Villarroya, R. Cereijo, and F. Villarroya, “An endocrine role for brown adipose tissue?,” *Am. J. Physiol. Endocrinol. Metab.*, vol. 305, no. 5, pp. E567-572, Sep. 2013.

[9] K. I. Stanford *et al.*, “Brown adipose tissue regulates glucose homeostasis and insulin sensitivity,” *J. Clin. Invest.*, vol. 123, no. 1, pp. 215–223, Jan. 2013.

[10] A. M. Cypess *et al.*, “Identification and importance of brown adipose tissue in adult humans,” *N. Engl. J. Med.*, vol. 360, no. 15, pp. 1509–1517, Apr. 2009.

[11] M. Saito *et al.*, “High incidence of metabolically active brown adipose tissue in healthy adult humans: effects of cold exposure and adiposity,” *Diabetes*, vol. 58, no. 7, pp. 1526–1531, Jul. 2009.

[12] D. Jaquet, A. Gaboriau, P. Czernichow, and C. Levy-Marchal, “Insulin resistance early in adulthood in subjects born with intrauterine growth retardation,” *J. Clin. Endocrinol. Metab.*, vol. 85, no. 4, pp. 1401–1406, Apr. 2000.

[13] D. Jaquet, S. Deghmoun, D. Chevenne, D. Collin, P. Czernichow, and C. Lévy-Marchal, “Dynamic change in adiposity from fetal to postnatal life is involved in the metabolic syndrome associated with reduced fetal growth,” *Diabetologia*, vol. 48, no. 5, pp. 849–855, May 2005.

[14] B. Muhlhausler and S. R. Smith, “Early-life origins of metabolic dysfunction: role of the adipocyte,” *Trends Endocrinol. Metab. TEM*, vol. 20, no. 2, pp. 51–57, Mar. 2009.

[15] M. H. Vickers, B. H. Breier, W. S. Cutfield, P. L. Hofman, and P. D. Gluckman, “Fetal origins of hyperphagia, obesity, and hypertension and

postnatal amplification by hypercaloric nutrition," *Am. J. Physiol. Endocrinol. Metab.*, vol. 279, no. 1, pp. E83-87, Jul. 2000.
[16] M. J. R. Heerwagen, M. R. Miller, L. A. Barbour, and J. E. Friedman, "Maternal obesity and fetal metabolic programming: a fertile epigenetic soil," *Am. J. Physiol. Regul. Integr. Comp. Physiol.*, vol. 299, no. 3, pp. R711-722, Sep. 2010.
[17] R. C. Andrews and B. R. Walker, "Glucocorticoids and insulin resistance: old hormones, new targets," *Clin. Sci. Lond. Engl. 1979*, vol. 96, no. 5, pp. 513–523, May 1999.
[18] S. Dube, M. Q. Slama, A. Basu, R. A. Rizza, and R. Basu, "Glucocorticoid Excess Increases Hepatic 11β-HSD-1 Activity in Humans: Implications in Steroid-Induced Diabetes," *J. Clin. Endocrinol. Metab.*, vol. 100, no. 11, pp. 4155–4162, Nov. 2015.
[19] D. Hutter, J. Kingdom, and E. Jaeggi, "Causes and mechanisms of intrauterine hypoxia and its impact on the fetal cardiovascular system: a review," *Int. J. Pediatr.*, vol. 2010, p. 401323, 2010.
[20] F. Westermeier, P. J. Sáez, R. Villalobos-Labra, L. Sobrevia, and M. Farías-Jofré, "Programming of fetal insulin resistance in pregnancies with maternal obesity by ER stress and inflammation," *BioMed Res. Int.*, vol. 2014, p. 917672, 2014.
[21] P. M. Williams and S. Fletcher, "Health effects of prenatal radiation exposure," *Am. Fam. Physician*, vol. 82, no. 5, pp. 488–493, Sep. 2010.
[22] L. Tomášová, B. Smajda, and J. Sevc, "Effects of prenatal irradiation on behaviour and hippocampal neurogenesis in adult rats," *Acta Physiol. Hung.*, vol. 99, no. 2, pp. 126–132, Jun. 2012.
[23] N. Kokošová, L. Tomášová, T. Kisková, and B. Šmajda, "Neuronal analysis and behaviour in prenatally gamma-irradiated rats," *Cell. Mol. Neurobiol.*, vol. 35, no. 1, pp. 45–55, Jan. 2015.
[24] T. Verreet *et al.*, "Persistent Impact of In utero Irradiation on Mouse Brain Structure and Function Characterized by MR Imaging and Behavioral Analysis," *Front. Behav. Neurosci.*, vol. 10, p. 83, 2016.
[25] J. Ye *et al.*, "Downregulating SOCS3 with siRNA ameliorates insulin signaling and glucose metabolism in hepatocytes of IUGR rats with catch-up growth," *Pediatr. Res.*, vol. 72, no. 6, pp. 550–559, Dec. 2012.
[26] O. Dumortier *et al.*, "Age-Dependent Control of Energy Homeostasis by Brown Adipose Tissue in Progeny Subjected to Maternal Diet-Induced Fetal Programming," *Diabetes*, vol. 66, no. 3, pp. 627–639, Mar. 2017.
[27] A. Bartelt *et al.*, "Brown adipose tissue activity controls triglyceride clearance," *Nat. Med.*, vol. 17, no. 2, pp. 200–205, Feb. 2011.
[28] S. Kooijman *et al.*, "Central GLP-1 receptor signalling accelerates plasma clearance of triacylglycerol and glucose by activating brown adipose tissue in mice," *Diabetologia*, vol. 58, no. 11, pp. 2637–2646, Nov. 2015.
[29] M. J. Nyirenda, R. S. Lindsay, C. J. Kenyon, A. Burchell, and J. R. Seckl, "Glucocorticoid exposure in late gestation permanently programs rat hepatic phosphoenolpyruvate carboxykinase and glucocorticoid receptor expression

and causes glucose intolerance in adult offspring," *J. Clin. Invest.*, vol. 101, no. 10, pp. 2174–2181, May 1998.
[30] M. Desai, C. D. Byrne, J. Zhang, C. J. Petry, A. Lucas, and C. N. Hales, "Programming of hepatic insulin-sensitive enzymes in offspring of rat dams fed a protein-restricted diet," *Am. J. Physiol.*, vol. 272, no. 5 Pt 1, pp. G1083-1090, May 1997.
[31] J. Boucher *et al.*, "Impaired thermogenesis and adipose tissue development in mice with fat-specific disruption of insulin and IGF-1 signalling," *Nat. Commun.*, vol. 3, p. 902, Jun. 2012.
[32] M. R. Mirbolooki, S. K. Upadhyay, C. C. Constantinescu, M.-L. Pan, and J. Mukherjee, "Adrenergic pathway activation enhances brown adipose tissue metabolism: a [^{18}F]FDG PET/CT study in mice," *Nucl. Med. Biol.*, vol. 41, no. 1, pp. 10–16, Jan. 2014.
[33] X. Wang and R. Wahl, "Responses of the insulin signaling pathways in the brown adipose tissue of rats following cold exposure," *PloS One*, vol. 9, no. 6, p. e99772, 2014.
[34] C. Wu *et al.*, "Activating brown adipose tissue for weight loss and lowering of blood glucose levels: a microPET study using obese and diabetic model mice," *PloS One*, vol. 9, no. 12, p. e113742, 2014.
[35] H. Selye, "Forty years of stress research: principal remaining problems and misconceptions," *Can. Med. Assoc. J.*, vol. 115, no. 1, pp. 53–56, Jul. 1976.
[36] A. Kapoor, E. Dunn, A. Kostaki, M. H. Andrews, and S. G. Matthews, "Fetal programming of hypothalamo-pituitary-adrenal function: prenatal stress and glucocorticoids," *J. Physiol.*, vol. 572, no. Pt 1, pp. 31–44, Apr. 2006.
[37] F. Xiong and L. Zhang, "Role of the hypothalamic-pituitary-adrenal axis in developmental programming of health and disease," *Front. Neuroendocrinol.*, vol. 34, no. 1, pp. 27–46, Jan. 2013.
[38] C. M. Boney, A. Verma, R. Tucker, and B. R. Vohr, "Metabolic syndrome in childhood: association with birth weight, maternal obesity, and gestational diabetes mellitus," *Pediatrics*, vol. 115, no. 3, pp. e290-296, Mar. 2005.
[39] D. R. McCance, D. J. Pettitt, R. L. Hanson, L. T. Jacobsson, W. C. Knowler, and P. H. Bennett, "Birth weight and non-insulin dependent diabetes: thrifty genotype, thrifty phenotype, or surviving small baby genotype?," *BMJ*, vol. 308, no. 6934, pp. 942–945, Apr. 1994.
[40] D. J. Barker, C. N. Hales, C. H. Fall, C. Osmond, K. Phipps, and P. M. Clark, "Type 2 (non-insulin-dependent) diabetes mellitus, hypertension and hyperlipidaemia (syndrome X): relation to reduced fetal growth," *Diabetologia*, vol. 36, no. 1, pp. 62–67, Jan. 1993.
[41] C. N. Hales and D. J. P. Barker, "Type 2 (non-insulin-dependent) diabetes mellitus: the thrifty phenotype hypothesis. 1992," *Int. J. Epidemiol.*, vol. 42, no. 5, pp. 1215–1222, Oct. 2013.
[42] C. L. White, M. N. Purpera, and C. D. Morrison, "Maternal obesity is necessary for programming effect of high-fat diet on offspring," *Am. J. Physiol. Regul. Integr. Comp. Physiol.*, vol. 296, no. 5, pp. R1464-1472, May 2009.

[43] R. Lakshmy, “Metabolic syndrome: role of maternal undernutrition and fetal programming,” *Rev. Endocr. Metab. Disord.*, vol. 14, no. 3, pp. 229–240, Sep. 2013.
[44] S. Zheng, M. Rollet, and Y.-X. Pan, “Maternal protein restriction during pregnancy induces CCAAT/enhancer-binding protein (C/EBPβ) expression through the regulation of histone modification at its promoter region in female offspring rat skeletal muscle,” *Epigenetics*, vol. 6, no. 2, pp. 161–170, Feb. 2011.
[45] D. E. Duque-Guimar es and S. E. Ozanne, “Nutritional programming of insulin resistance: causes and consequences,” *Trends Endocrinol. Metab. TEM*, vol. 24, no. 10, pp. 525–535, Oct. 2013.
[46] P. D. Taylor *et al.*, “Impaired glucose homeostasis and mitochondrial abnormalities in offspring of rats fed a fat-rich diet in pregnancy,” *Am. J. Physiol. Regul. Integr. Comp. Physiol.*, vol. 288, no. 1, pp. R134-139, Jan. 2005.
[47] M. Srinivasan, S. D. Katewa, A. Palaniyappan, J. D. Pandya, and M. S. Patel, “Maternal high-fat diet consumption results in fetal malprogramming predisposing to the onset of metabolic syndrome-like phenotype in adulthood,” *Am. J. Physiol. Endocrinol. Metab.*, vol. 291, no. 4, pp. E792-799, Oct. 2006.
[48] N. G. Ashino *et al.*, “Maternal high-fat feeding through pregnancy and lactation predisposes mouse offspring to molecular insulin resistance and fatty liver,” *J. Nutr. Biochem.*, vol. 23, no. 4, pp. 341–348, Apr. 2012.
[49] A. Dudele *et al.*, “Chronic maternal inflammation or high-fat-feeding programs offspring obesity in a sex-dependent manner,” *Int. J. Obes. 2005*, vol. 41, no. 9, pp. 1420–1426, Sep. 2017.
[50] J. C. Kingdom and P. Kaufmann, “Oxygen and placental villous development: origins of fetal hypoxia,” *Placenta*, vol. 18, no. 8, pp. 613-621-626, Nov. 1997.
[51] G. M. Jensen and L. G. Moore, “The effect of high altitude and other risk factors on birthweight: independent or interactive effects?,” *Am. J. Public Health*, vol. 87, no. 6, pp. 1003–1007, Jun. 1997.
[52] F. L. Lueder, S. B. Kim, C. A. Buroker, S. A. Bangalore, and E. S. Ogata, “Chronic maternal hypoxia retards fetal growth and increases glucose utilization of select fetal tissues in the rat,” *Metabolism.*, vol. 44, no. 4, pp. 532–537, Apr. 1995.
[53] L. G. Moore, “Fetal growth restriction and maternal oxygen transport during high altitude pregnancy,” *High Alt. Med. Biol.*, vol. 4, no. 2, pp. 141–156, 2003.
[54] S. M. Smith and W. W. Vale, “The role of the hypothalamic-pituitary-adrenal axis in neuroendocrine responses to stress,” *Dialogues Clin. Neurosci.*, vol. 8, no. 4, pp. 383–395, 2006.
[55] E. T. Uchoa, G. Aguilera, J. P. Herman, J. L. Fiedler, T. Deak, and M. B. C. de Sousa, “Novel aspects of glucocorticoid actions,” *J. Neuroendocrinol.*, vol. 26, no. 9, pp. 557–572, Sep. 2014.

[56] M. K. Hankir *et al.*, “Dissociation Between Brown Adipose Tissue18F-FDG Uptake and Thermogenesis in Uncoupling Protein 1-Deficient Mice,” *J. Nucl. Med. Off. Publ. Soc. Nucl. Med.*, vol. 58, no. 7, pp. 1100–1103, Jul. 2017.
[57] R. P. Jensh and R. L. Brent, “Effects of 0.6-Gy prenatal X irradiation on postnatal neurophysiologic development in the Wistar rat,” *Proc. Soc. Exp. Biol. Med. Soc. Exp. Biol. Med. N. Y. N*, vol. 181, no. 4, pp. 611–619, Apr. 1986.
[58] R. P. Jensh, R. L. Brent, and W. H. Vogel, “Studies concerning the effects of low level prenatal X-irradiation on postnatal growth and adult behaviour in the Wistar rat,” *Int. J. Radiat. Biol. Relat. Stud. Phys. Chem. Med.*, vol. 50, no. 6, pp. 1069–1081, Dec. 1986.
[59] R. Baskar and P. U. Devi, “Long-term effect of prenatal exposure to low level of gamma radiation on neurophysiology of mouse,” *Indian J. Exp. Biol.*, vol. 34, no. 9, pp. 887–890, Sep. 1996.
[60] J. W. Wood, K. G. Johnson, and Y. Omori, “In utero exposure to the Hiroshima atomic bomb. An evaluation of head size and mental retardation: twenty years later,” *Pediatrics*, vol. 39, no. 3, pp. 385–392, Mar. 1967.
[61] J. A. Reisz, N. Bansal, J. Qian, W. Zhao, and C. M. Furdui, “Effects of ionizing radiation on biological molecules--mechanisms of damage and emerging methods of detection,” *Antioxid. Redox Signal.*, vol. 21, no. 2, pp. 260–292, Jul. 2014.
[62] S. Tharmalingam, S. Sreetharan, A. V. Kulesza, D. R. Boreham, and T. C. Tai, “Low-Dose Ionizing Radiation Exposure, Oxidative Stress and Epigenetic Programing of Health and Disease,” *Radiat. Res.*, vol. 188, no. 4.2, pp. 525–538, 2017.
[63] H.-S. Lee, “Impact of Maternal Diet on the Epigenome during In Utero Life and the Developmental Programming of Diseases in Childhood and Adulthood,” *Nutrients*, vol. 7, no. 11, pp. 9492–9507, Nov. 2015.
[64] L. S. Branch, “Consolidated federal laws of canada, Radiation Protection Regulations,” 22-Sep-2017. [Online]. Available: http://laws-lois.justice.gc.ca/eng/regulations/SOR-2000-203/. [Accessed: 01-Mar-2018].
[65] “United Nations Scientific Committee on the Effects of Atomic Radiation. Effects of ionizing radiation. Volume 1, UNSCEAR 2008 report to the General Assembly, with scientific annexes.,” New York, 2008.
[66] C. L. Sanders, *Radiation hormesis and the linear-no-threshold assumption*. Heidelberg: Springer, 2010.
[67] C. N. Safety Commission, “Radiation Health Effects,” 03-Feb-2014. [Online]. Available: http://nuclearsafety.gc.ca/eng/resources/radiation/introduction-to-radiation/radiation-health-effects.cfm. [Accessed: 24-Feb-2018].
[68] R. E. J. Mitchel, “Adaption By Low Dose Radiation Exposure: A Look at Scope and Limitations for Radioprotection,” *Dose-Response Publ. Int. Hormesis Soc.*, vol. 13, no. 1, Mar. 2015.
[69] R. E. J. Mitchel, “Low doses of radiation are protective in vitro and in vivo: evolutionary origins,” *Dose-Response Publ. Int. Hormesis Soc.*, vol. 4, no. 2, pp. 75–90, Aug. 2006.

[70] “United Nations Scientific Committee on the Sources, effects and risks of ionizing radiation. Annex A: Levels and effects of radiation exposure due to the nuclear accident after the 2011 great east-Japan earthquake and tsunami.,” New York, 2014.
[71] D. Grahn and K. F. Hamilton, “Genetic Variation in the Acute Lethal Response of Four Inbred Mouse Strains to Whole Body X-Irradiation,” *Genetics*, vol. 42, no. 3, pp. 189–198, May 1957.
[72] R. H. Mole, “The LD50 for uniform low LET irradiation of man,” *Br. J. Radiol.*, vol. 57, no. 677, pp. 355–369, May 1984.
[73] R. W. Miller, “Effects of prenatal exposure to ionizing radiation,” *Health Phys.*, vol. 59, no. 1, pp. 57–61, Jul. 1990.
[74] C. Streffer *et al.*, “Biological effects after prenatal irradiation (embryo and fetus). A report of the International Commission on Radiological Protection,” *Ann. ICRP*, vol. 33, no. 1–2, pp. 5–206, 2003.
[75] L. B. Russell and W. L. Russell, “The effect of radiation on the preimplantation stages of the mouse embryo.,” *Anat. Rec.*, vol. 108, p. 521, 1950.
[76] L. B. Russell, “X-ray-induced developmental abnormalities in the mouse and their use in the analysis of embryological patterns. II. Abnormalities of the vertebral column and thorax.,” *J. Exp. Zool.*, vol. 131, pp. 329–395, 1956.
[77] B. S. Heyer, A. MacAuley, O. Behrendtsen, and Z. Werb, “Hypersensitivity to DNA damage leads to increased apoptosis during early mouse development,” *Genes Dev.*, vol. 14, no. 16, pp. 2072–2084, Aug. 2000.
[78] P. Jacquet, “Sensitivity of germ cells and embryos to ionizing radiation,” *J. Biol. Regul. Homeost. Agents*, vol. 18, no. 2, pp. 106–114, Jun. 2004.
[79] M. De Santis, E. Cesari, E. Nobili, G. Straface, A. F. Cavaliere, and A. Caruso, “Radiation effects on development,” *Birth Defects Res. Part C Embryo Today Rev.*, vol. 81, no. 3, pp. 177–182, Sep. 2007.
[80] P. Shaw, A. Duncan, A. Vouyouka, and K. Ozsvath, “Radiation exposure and pregnancy,” *J. Vasc. Surg.*, vol. 53, no. 1 Suppl, p. 28S–34S, Jan. 2011.
[81] J. A. Falch, “[Can substitution therapy with thyroxine cause osteoporosis?],” *Tidsskr. Den Nor. Laegeforening Tidsskr. Prakt. Med. Ny Raekke*, vol. 112, no. 2, pp. 260–261, Jan. 1992.
[82] L. E. Young, “Imprinting of genes and the Barker hypothesis,” *Twin Res. Off. J. Int. Soc. Twin Stud.*, vol. 4, no. 5, pp. 307–317, Oct. 2001.
[83] A. A. Jackson, “Nutrients, growth, and the development of programmed metabolic function,” *Adv. Exp. Med. Biol.*, vol. 478, pp. 41–55, 2000.
[84] R. W. Miller, “Delayed effects occurring within the first decade after exposure of young individuals to the Hiroshima atomic bomb,” *Pediatrics*, vol. 18, no. 1, pp. 1–18, Jul. 1956.
[85] W. C. Moloney and M. A. Kastenbaum, “Leukemogenic effects of ionizing radiation on atomic bomb survivors in Hiroshima City,” *Science*, vol. 121, no. 3139, pp. 308–309, Feb. 1955.
[86] M. Otake and W. J. Schull, “Radiation-related small head sizes among prenatally exposed A-bomb survivors,” *Int. J. Radiat. Biol.*, vol. 63, no. 2, pp. 255–270, Feb. 1993.

[87] M. Rahu, “Health effects of the Chernobyl accident: fears, rumours and the truth,” *Eur. J. Cancer Oxf. Engl. 1990*, vol. 39, no. 3, pp. 295–299, Feb. 2003.
[88] D. J. Brenner and E. J. Hall, “Computed tomography--an increasing source of radiation exposure,” *N. Engl. J. Med.*, vol. 357, no. 22, pp. 2277–2284, Nov. 2007.
[89] E. J. Hall and D. J. Brenner, “Cancer risks from diagnostic radiology: the impact of new epidemiological data,” *Br. J. Radiol.*, vol. 85, no. 1020, pp. e1316-1317, Dec. 2012.
[90] K. Leuraud *et al.*, “Ionising radiation and risk of death from leukaemia and lymphoma in radiation-monitored workers (INWORKS): an international cohort study,” *Lancet Haematol.*, vol. 2, no. 7, pp. e276-281, Jul. 2015.
[91] P. Steenvoorde, E. K. Pauwels, L. K. Harding, M. Bourguignon, B. Marière, and J. J. Broerse, “Diagnostic nuclear medicine and risk for the fetus,” *Eur. J. Nucl. Med.*, vol. 25, no. 2, pp. 193–199, Feb. 1998.
[92] M. Hossain and P. Uma Devi, “Effect of irradiation at the early foetal stage on adult brain function of mouse: learning and memory,” *Int. J. Radiat. Biol.*, vol. 77, no. 5, pp. 581–585, May 2001.
[93] M. Hossain, M. Chetana, and P. U. Devi, “Late effect of prenatal irradiation on the hippocampal histology and brain weight in adult mice,” *Int. J. Dev. Neurosci. Off. J. Int. Soc. Dev. Neurosci.*, vol. 23, no. 4, pp. 307–313, Jun. 2005.
[94] M. Hossain and P. Uma Devi, “Effect of irradiation at the early fetal stage on adult brain function in the mouse: locomotor activity,” *Int. J. Radiat. Biol.*, vol. 76, no. 10, pp. 1397–1402, Oct. 2000.
[95] P. U. Devi and M. Hossain, “Induction of chromosomal instability in mouse hemopoietic cells by fetal irradiation,” *Mutat. Res.*, vol. 456, no. 1–2, pp. 33–37, Nov. 2000.
[96] T. Minamisawa, K. Hirokaga, and S. Sasaki, “Gross morphological changes of the mouse brain exposed prenatally to ionizing radiation,” *J. Radiat. Res. (Tokyo)*, vol. 31, no. 2, pp. 214–218, Jun. 1990.
[97] P. U. Devi, M. Hossain, and K. S. Bisht, “Effect of late fetal irradiation on adult behavior of mouse: Dose-response relationship,” *Neurotoxicol. Teratol.*, vol. 21, no. 2, pp. 193–198, Apr. 1999.
[98] T. Minamisawa and K. Hirokaga, “Long term effects of prenatal exposure to low level gamma rays on spontaneous circadian motor activity of male mice,” *J. Radiat. Res. (Tokyo)*, vol. 36, no. 3, pp. 179–184, Sep. 1995.
[99] T. Minamisawa and K. Hirokaga, “Long-term effects of prenatal exposure to low levels of gamma rays on open-field activity in male mice,” *Radiat. Res.*, vol. 144, no. 2, pp. 237–240, Nov. 1995.
[100] M. Hossain, P. U. Devi, and K. S. Bisht, “Effect of prenatal gamma irradiation during the late fetal period on the postnatal development of the mouse,” *Teratology*, vol. 59, no. 3, pp. 133–138, Mar. 1999.
[101] J. M. Heaton, “The distribution of brown adipose tissue in the human,” *J. Anat.*, vol. 112, no. Pt 1, pp. 35–39, May 1972.

[102] R. Hao, L. Yuan, N. Zhang, C. Li, and J. Yang, “Brown adipose tissue: distribution and influencing factors on FDG PET/CT scan,” *J. Pediatr. Endocrinol. Metab. JPEM*, vol. 25, no. 3–4, pp. 233–237, 2012.
[103] M. J. Vosselman, W. D. van Marken Lichtenbelt, and P. Schrauwen, “Energy dissipation in brown adipose tissue: from mice to men,” *Mol. Cell. Endocrinol.*, vol. 379, no. 1–2, pp. 43–50, Oct. 2013.
[104] D. Richard, A. C. Carpentier, G. Doré, V. Ouellet, and F. Picard, “Determinants of brown adipocyte development and thermogenesis,” *Int. J. Obes. 2005*, vol. 34 Suppl 2, pp. S59-66, Dec. 2010.
[105] D. G. Nicholls and R. M. Locke, “Thermogenic mechanisms in brown fat,” *Physiol. Rev.*, vol. 64, no. 1, pp. 1–64, Jan. 1984.
[106] C. Porter, “Quantification of UCP1 function in human brown adipose tissue,” *Adipocyte*, vol. 6, no. 2, pp. 167–174, Apr. 2017.
[107] D. Richard and F. Picard, “Brown fat biology and thermogenesis,” *Front. Biosci. Landmark Ed.*, vol. 16, pp. 1233–1260, Jan. 2011.
[108] B. Cannon and J. Nedergaard, “Brown adipose tissue: function and physiological significance,” *Physiol. Rev.*, vol. 84, no. 1, pp. 277–359, Jan. 2004.
[109] M. Klingenberg and S. G. Huang, “Structure and function of the uncoupling protein from brown adipose tissue,” *Biochim. Biophys. Acta*, vol. 1415, no. 2, pp. 271–296, Jan. 1999.
[110] D. G. Nicholls, “The physiological regulation of uncoupling proteins,” *Biochim. Biophys. Acta*, vol. 1757, no. 5–6, pp. 459–466, Jun. 2006.
[111] A. S. Divakaruni and M. D. Brand, “The regulation and physiology of mitochondrial proton leak,” *Physiol. Bethesda Md*, vol. 26, no. 3, pp. 192–205, Jun. 2011.
[112] W. Cao, A. V. Medvedev, K. W. Daniel, and S. Collins, “beta-Adrenergic activation of p38 MAP kinase in adipocytes: cAMP induction of the uncoupling protein 1 (UCP1) gene requires p38 MAP kinase,” *J. Biol. Chem.*, vol. 276, no. 29, pp. 27077–27082, Jul. 2001.
[113] S. Collins, K. W. Daniel, A. E. Petro, and R. S. Surwit, “Strain-specific response to beta 3-adrenergic receptor agonist treatment of diet-induced obesity in mice,” *Endocrinology*, vol. 138, no. 1, pp. 405–413, Jan. 1997.
[114] A. Géloën, A. J. Collet, G. Guay, and L. J. Bukowiecki, “Beta-adrenergic stimulation of brown adipocyte proliferation,” *Am. J. Physiol.*, vol. 254, no. 1 Pt 1, pp. C175-182, Jan. 1988.
[115] M. R. Mirbolooki, C. C. Constantinescu, M.-L. Pan, and J. Mukherjee, “Quantitative assessment of brown adipose tissue metabolic activity and volume using 18F-FDG PET/CT and β3-adrenergic receptor activation,” *EJNMMI Res.*, vol. 1, no. 1, p. 30, Dec. 2011.
[116] H. M. Feldmann, V. Golozoubova, B. Cannon, and J. Nedergaard, “UCP1 ablation induces obesity and abolishes diet-induced thermogenesis in mice exempt from thermal stress by living at thermoneutrality,” *Cell Metab.*, vol. 9, no. 2, pp. 203–209, Feb. 2009.

[117] S. Kooijman, J. K. van den Heuvel, and P. C. N. Rensen, “Neuronal Control of Brown Fat Activity,” *Trends Endocrinol. Metab. TEM*, vol. 26, no. 11, pp. 657–668, Nov. 2015.
[118] T. J. Bartness, C. H. Vaughan, and C. K. Song, “Sympathetic and sensory innervation of brown adipose tissue,” *Int. J. Obes. 2005*, vol. 34 Suppl 1, pp. S36-42, Oct. 2010.
[119] M. Chondronikola *et al.*, “Brown adipose tissue improves whole-body glucose homeostasis and insulin sensitivity in humans,” *Diabetes*, vol. 63, no. 12, pp. 4089–4099, Dec. 2014.
[120] D. A. Cross, D. R. Alessi, P. Cohen, M. Andjelkovich, and B. A. Hemmings, “Inhibition of glycogen synthase kinase-3 by insulin mediated by protein kinase B,” *Nature*, vol. 378, no. 6559, pp. 785–789, Dec. 1995.
[121] H. Eldar-Finkelman, S. A. Schreyer, M. M. Shinohara, R. C. LeBoeuf, and E. G. Krebs, “Increased glycogen synthase kinase-3 activity in diabetes- and obesity-prone C57BL/6J mice,” *Diabetes*, vol. 48, no. 8, pp. 1662–1666, Aug. 1999.
[122] S. E. Nikoulina, T. P. Ciaraldi, S. Mudaliar, P. Mohideen, L. Carter, and R. R. Henry, “Potential role of glycogen synthase kinase-3 in skeletal muscle insulin resistance of type 2 diabetes,” *Diabetes*, vol. 49, no. 2, pp. 263–271, Feb. 2000.
[123] C. Cohade, K. A. Mourtzikos, and R. L. Wahl, “‘USA-Fat’: prevalence is related to ambient outdoor temperature-evaluation with 18F-FDG PET/CT,” *J. Nucl. Med. Off. Publ. Soc. Nucl. Med.*, vol. 44, no. 8, pp. 1267–1270, Aug. 2003.
[124] Z. Glick, S. Y. Wu, J. Lupien, R. Reggio, G. A. Bray, and D. A. Fisher, “Meal-induced brown fat thermogenesis and thyroid hormone metabolism in rats,” *Am. J. Physiol.*, vol. 249, no. 5 Pt 1, pp. E519-524, Nov. 1985.
[125] M. Calderon-Dominguez, J. F. Mir, R. Fucho, M. Weber, D. Serra, and L. Herrero, “Fatty acid metabolism and the basis of brown adipose tissue function,” *Adipocyte*, vol. 5, no. 2, pp. 98–118, Jun. 2016.
[126] A. M. Cypess and C. R. Kahn, “Brown fat as a therapy for obesity and diabetes,” *Curr. Opin. Endocrinol. Diabetes Obes.*, vol. 17, no. 2, pp. 143–149, Apr. 2010.
[127] G. I. Shulman, “Cellular mechanisms of insulin resistance,” *J. Clin. Invest.*, vol. 106, no. 2, pp. 171–176, Jul. 2000.
[128] C. K. Roberts, A. L. Hevener, and R. J. Barnard, “Metabolic syndrome and insulin resistance: underlying causes and modification by exercise training,” *Compr. Physiol.*, vol. 3, no. 1, pp. 1–58, Jan. 2013.
[129] H. E. Lebovitz, “Insulin resistance: definition and consequences,” *Exp. Clin. Endocrinol. Diabetes Off. J. Ger. Soc. Endocrinol. Ger. Diabetes Assoc.*, vol. 109 Suppl 2, pp. S135-148, 2001.
[130] D. W. Lam and D. LeRoith, “Metabolic Syndrome,” in *Endotext*, L. J. De Groot, G. Chrousos, K. Dungan, K. R. Feingold, A. Grossman, J. M. Hershman, C. Koch, M. Korbonits, R. McLachlan, M. New, J. Purnell, R. Rebar, F. Singer, and A. Vinik, Eds. South Dartmouth (MA): MDText.com, Inc., 2000.

[131] Y. Kawano and D. E. Cohen, “Mechanisms of hepatic triglyceride accumulation in non-alcoholic fatty liver disease,” *J. Gastroenterol.*, vol. 48, no. 4, pp. 434–441, Apr. 2013.
[132] Z. Gong, E. Tas, S. Yakar, and R. Muzumdar, “Hepatic lipid metabolism and non-alcoholic fatty liver disease in aging,” *Mol. Cell. Endocrinol.*, vol. 455, pp. 115–130, Nov. 2017.
[133] N. Gruben, R. Shiri-Sverdlov, D. P. Y. Koonen, and M. H. Hofker, “Nonalcoholic fatty liver disease: A main driver of insulin resistance or a dangerous liaison?,” *Biochim. Biophys. Acta*, vol. 1842, no. 11, pp. 2329–2343, Nov. 2014.
[134] P. W. Miller, N. J. Long, R. Vilar, and A. D. Gee, “Synthesis of 11C, 18F, 15O, and 13N radiolabels for positron emission tomography,” *Angew. Chem. Int. Ed Engl.*, vol. 47, no. 47, pp. 8998–9033, 2008.
[135] S. Garbarino *et al.*, “A new compartmental method for the analysis of liver FDG kinetics in small animal models,” *EJNMMI Res.*, vol. 5, no. 1, p. 107, Dec. 2015.
[136] A. Almuhaideb, N. Papathanasiou, and J. Bomanji, “18F-FDG PET/CT imaging in oncology,” *Ann. Saudi Med.*, vol. 31, no. 1, pp. 3–13, Feb. 2011.
[137] J. Nedergaard, T. Bengtsson, and B. Cannon, “Unexpected evidence for active brown adipose tissue in adult humans,” *Am. J. Physiol. Endocrinol. Metab.*, vol. 293, no. 2, pp. E444-452, Aug. 2007.
[138] J. M. Olsen *et al.*, “β3-Adrenergically induced glucose uptake in brown adipose tissue is independent of UCP1 presence or activity: Mediation through the mTOR pathway,” *Mol. Metab.*, vol. 6, no. 6, pp. 611–619, Jun. 2017.
[139] K. Inokuma, Y. Ogura-Okamatsu, C. Toda, K. Kimura, H. Yamashita, and M. Saito, “Uncoupling protein 1 is necessary for norepinephrine-induced glucose utilization in brown adipose tissue,” *Diabetes*, vol. 54, no. 5, pp. 1385–1391, May 2005.
[140] L. Pace *et al.*, “Determinants of physiologic 18F-FDG uptake in brown adipose tissue in sequential PET/CT examinations,” *Mol. Imaging Biol. MIB Off. Publ. Acad. Mol. Imaging*, vol. 13, no. 5, pp. 1029–1035, Oct. 2011.
[141] M. Saito *et al.*, “High incidence of metabolically active brown adipose tissue in healthy adult humans: effects of cold exposure and adiposity,” *Diabetes*, vol. 58, no. 7, pp. 1526–1531, Jul. 2009.
[142] M. J. W. Hanssen *et al.*, “Glucose uptake in human brown adipose tissue is impaired upon fasting-induced insulin resistance,” *Diabetologia*, vol. 58, no. 3, pp. 586–595, Mar. 2015.
[143] J. E. Gilda and A. V. Gomes, “Stain-Free total protein staining is a superior loading control to β-actin for Western blots,” *Anal. Biochem.*, vol. 440, no. 2, pp. 186–188, Sep. 2013.
[144] C. N. Hales *et al.*, “Fetal and infant growth and impaired glucose tolerance at age 64,” *BMJ*, vol. 303, no. 6809, pp. 1019–1022, Oct. 1991.
[145] J.M. Wit and B. Boersma, “Catch-up growth: definition, mechanisms, and models,” *J. Pediatr. Endocrinol. Metab. JPEM*, vol. 15 Suppl 5, pp. 1229–1241, Dec. 2002.

[146] K. K. S. Bhasin, A. van Nas, L. J. Martin, R. C. Davis, S. U. Devaskar, and A. J. Lusis, “Maternal low-protein diet or hypercholesterolemia reduces circulating essential amino acids and leads to intrauterine growth restriction,” *Diabetes*, vol. 58, no. 3, pp. 559–566, Mar. 2009.
[147] J. C. Jimenez-Chillaron *et al.*, “Reductions in caloric intake and early postnatal growth prevent glucose intolerance and obesity associated with low birthweight,” *Diabetologia*, vol. 49, no. 8, pp. 1974–1984, Aug. 2006.
[148] K. K. Ong, M. L. Ahmed, P. M. Emmett, M. A. Preece, and D. B. Dunger, “Association between postnatal catch-up growth and obesity in childhood: prospective cohort study,” *BMJ*, vol. 320, no. 7240, pp. 967–971, Apr. 2000.
[149] L. Ibáñez, K. Ong, D. B. Dunger, and F. de Zegher, “Early development of adiposity and insulin resistance after catch-up weight gain in small-for-gestational-age children,” *J. Clin. Endocrinol. Metab.*, vol. 91, no. 6, pp. 2153–2158, Jun. 2006.
[150] S. M. Muaku, J. P. Thissen, G. Gerard, J. M. Ketelslegers, and D. Maiter, “Postnatal catch-up growth induced by growth hormone and insulin-like growth factor-I in rats with intrauterine growth retardation caused by maternal protein malnutrition,” *Pediatr. Res.*, vol. 42, no. 3, pp. 370–377, Sep. 1997.
[151] S.H. Koo, “Nonalcoholic fatty liver disease: molecular mechanisms for the hepatic steatosis,” *Clin. Mol. Hepatol.*, vol. 19, no. 3, pp. 210–215, Sep. 2013.
[152] H. C. Masuoka and N. Chalasani, “Nonalcoholic fatty liver disease: an emerging threat to obese and diabetic individuals,” *Ann. N. Y. Acad. Sci.*, vol. 1281, pp. 106–122, Apr. 2013.
[153] J. L. Sarvas, N. Khaper, and S. J. Lees, “The IL-6 Paradox: Context Dependent Interplay of SOCS3 and AMPK,” *J. Diabetes Metab.*, vol. Suppl 13, May 2013.
[154] K. Ueki, T. Kondo, and C. R. Kahn, “Suppressor of cytokine signaling 1 (SOCS-1) and SOCS-3 cause insulin resistance through inhibition of tyrosine phosphorylation of insulin receptor substrate proteins by discrete mechanisms,” *Mol. Cell. Biol.*, vol. 24, no. 12, pp. 5434–5446, Jun. 2004.
[155] L. Rui, M. Yuan, D. Frantz, S. Shoelson, and M. F. White, “SOCS-1 and SOCS-3 block insulin signaling by ubiquitin-mediated degradation of IRS1 and IRS2,” *J. Biol. Chem.*, vol. 277, no. 44, pp. 42394–42398, Nov. 2002.
[156] K. Ueki, T. Kadowaki, and C. R. Kahn, “Role of suppressors of cytokine signaling SOCS-1 and SOCS-3 in hepatic steatosis and the metabolic syndrome,” *Hepatol. Res. Off. J. Jpn. Soc. Hepatol.*, vol. 33, no. 2, pp. 185–192, Oct. 2005.
[157] J. Yang, S. C. Kalhan, and R. W. Hanson, “What is the metabolic role of phosphoenolpyruvate carboxykinase?,” *J. Biol. Chem.*, vol. 284, no. 40, pp. 27025–27029, Oct. 2009.
[158] A. Valera, A. Pujol, M. Pelegrin, and F. Bosch, “Transgenic mice overexpressing phosphoenolpyruvate carboxykinase develop non-insulin-dependent diabetes mellitus,” *Proc. Natl. Acad. Sci. U. S. A.*, vol. 91, no. 19, pp. 9151–9154, Sep. 1994.

[159] P. G. Quinn and D. Yeagley, “Insulin regulation of PEPCK gene expression: a model for rapid and reversible modulation,” *Curr. Drug Targets Immune Endocr. Metab. Disord.*, vol. 5, no. 4, pp. 423–437, Dec. 2005.
[160] M. D. Michael *et al.*, “Loss of insulin signaling in hepatocytes leads to severe insulin resistance and progressive hepatic dysfunction,” *Mol. Cell*, vol. 6, no. 1, pp. 87–97, Jul. 2000.
[161] Y. Sun *et al.*, “Phosphoenolpyruvate carboxykinase overexpression selectively attenuates insulin signaling and hepatic insulin sensitivity in transgenic mice,” *J. Biol. Chem.*, vol. 277, no. 26, pp. 23301–23307, Jun. 2002.
[162] S. M. Labbé *et al.*, “In vivo measurement of energy substrate contribution to cold-induced brown adipose tissue thermogenesis,” *FASEB J. Off. Publ. Fed. Am. Soc. Exp. Biol.*, vol. 29, no. 5, pp. 2046–2058, May 2015.
[163] W. A. Banks *et al.*, “Triglycerides induce leptin resistance at the blood-brain barrier,” *Diabetes*, vol. 53, no. 5, pp. 1253–1260, May 2004.
[164] M. G. Myers, R. L. Leibel, R. J. Seeley, and M. W. Schwartz, “Obesity and leptin resistance: distinguishing cause from effect,” *Trends Endocrinol. Metab. TEM*, vol. 21, no. 11, pp. 643–651, Nov. 2010.
[165] P. B. Jakus, A. Sandor, T. Janaky, and V. Farkas, “Cooperation between BAT and WAT of rats in thermogenesis in response to cold, and the mechanism of glycogen accumulation in BAT during reacclimation,” *J. Lipid Res.*, vol. 49, no. 2, pp. 332–339, Feb. 2008.
[166] A. Benekou, S. Bolaris, E. Kazanis, E. Bozas, H. Philippidis, and F. Stylianopoulou, “In utero radiation-induced changes in growth factor levels in the developing rat brain,” *Int. J. Radiat. Biol.*, vol. 77, no. 1, pp. 83–93, Jan. 2001.
[167] P. Nguyen *et al.*, “Prenatal glucocorticoid exposure programs adrenal PNMT expression and adult hypertension,” *J. Endocrinol.*, vol. 227, no. 2, pp. 117–127, Nov. 2015.
[168] A. C. Huizink, P. G. Robles de Medina, E. J. H. Mulder, G. H. A. Visser, and J. K. Buitelaar, “Stress during pregnancy is associated with developmental outcome in infancy,” *J. Child Psychol. Psychiatry*, vol. 44, no. 6, pp. 810–818, Sep. 2003.
[169] A.-M. Samuelsson *et al.*, “Diet-induced obesity in female mice leads to offspring hyperphagia, adiposity, hypertension, and insulin resistance: a novel murine model of developmental programming,” *Hypertens. Dallas Tex 1979*, vol. 51, no. 2, pp. 383–392, Feb. 2008.
[170] J. M. Berg, J. L. Tymoczko, and L. Stryer, *Food Intake and Starvation Induce Metabolic Changes*. 2002.
[171] D. V. Rayner, “The sympathetic nervous system in white adipose tissue regulation,” *Proc. Nutr. Soc.*, vol. 60, no. 3, pp. 357–364, Aug. 2001.
[172] D. Grigore, N. B. Ojeda, and B. T. Alexander, “Sex differences in the fetal programming of hypertension,” *Gend. Med.*, vol. 5 Suppl A, pp. S121-132, 2008.
[173] D. O’Regan, C. J. Kenyon, J. R. Seckl, and M. C. Holmes, “Glucocorticoid exposure in late gestation in the rat permanently programs gender-specific

differences in adult cardiovascular and metabolic physiology," *Am. J. Physiol. Endocrinol. Metab.*, vol. 287, no. 5, pp. E863-870, Nov. 2004.
[174] M. Shen and H. Shi, "Sex Hormones and Their Receptors Regulate Liver Energy Homeostasis," *Int. J. Endocrinol.*, vol. 2015, pp. 294278, 2015.
[175] L. Fernández-Pérez, B. Guerra, J. C. Díaz-Chico, and A. Flores-Morales, "Estrogens regulate the hepatic effects of growth hormone, a hormonal interplay with multiple fates," *Front. Endocrinol.*, vol. 4, pp. 66, 2013.
[176] K. Staley and H. Scharfman, "A woman's prerogative," *Nat. Neurosci.*, vol. 8, no. 6, pp. 697–699, 2005.
[177] J. D. Neill and E. Knobil, Eds., *Knobil and Neill's physiology of reproduction*, vol. 2. Raven Press, New York, 1994.

Chapter 9. Appendix

9.1 List of Abbreviations

Akt – protein kinase B

ATP – adenosine triphosphate

BAT – brown adipose tissue

BMI – body mass index

cAMP – cyclic adenosine monophosphate

^{18}F-FDG – ^{18}F-flurodeoxyglucose

FSH – follicle-stimulating hormone

GH – growth hormone

GSK3β – glycogen synthase kinase 3 beta

HPA – hypothalamic-pituitary-adrenal

IBAT – interscapular brown adipose tissue

IRS – insulin receptor substrates

IRS-1 – insulin receptor 1

IRS-2 – insulin receptor 2

IUGR – intrauterine growth restriction

LDR – low dose radiation

LH – luteinizing hormone

NAFLD – non-alcoholic fatty liver disease

pAkt – phosphorylated protein kinase B

PET – positron emission tomography

pGSK3β - phosphorylated glycogen synthase kinase 3 beta

PKA – protein kinase A

SOCS3 – suppressor of cytokine signaling 3

SUV_{MAX} – maximum standardized uptake value

PEPCK – phosphoenolpyruvate carboxykinase

PI3K – phosphatidylinositol 3-kinase

SLDR – sub-lethal dose radiation

UCP1 – uncoupling protein 1

WAT – white adipose tissue

9.2 FDG Dilution Calculations

1. Measure activity of received sample. If in a vial, transfer to a syringe.
2. Obtain concentration based on the activity measurement and volume (µCi/ml).
3. Want final concentration of 300µCi/ml. Determine saline volume and FDG volume to acquire the desired concentration. C_i (µCi/ml) V_i (ml) = C_f (300 µCi/ml) V_f (1ml)

Ex. To make 1 ml at 300uCi/ml:

$1180\mu Ci/ml \times V_i = 300\mu Ci/ml \times 1ml$

$V_i = 300\mu Ci / 1180\mu Ci/ml$

4. With a new syringe take up saline volume first (1000µl-V_i) and then the FDG volume (V_i).
5. Eject this into a new eppendorf tube and take up into the syringe again for injection.
6. Check actual activity (concentration) present and determine amount to inject 20µCi into the mouse.

9.3 Western Blot SOP: Lees Lab

Day 1 - Gel Preparation and Running

What you need:
-gel apparatus with sponges (bench)
-glass plates (2 sized (1.5mm), 2 short plates) (bench)
-2 green plate holders (bench)
-combs same size as glass plates (bench)
-2x 50mL beakers (bench)
-1x 50mL tube
-10ml serological pipettes
-2 transfer pipettes
-Distilled water (DW)
-1.5M Tris pH 8.8 (4^{o}C)
-0.5M Tris pH 6.8 (4^{o}C)
-10% SDS (bench)
-40% acrylamide (4^{o}C)
-Ammonium persulfate (APS, 4^{o}C)
-TEMED (chemical storage cabinet)
-20% methanol (bench)
-0.1% SDS (bench)
-standard ladder (molecular marker) (-20^{o}C)
-gel running apparatus and container (bench)
-10ml syringe with needle

First remove samples from -80^{o}C to thaw on ice. If a white precipitate is present after thawing, place samples at 37^{o}C (using a heat block) until they are clear. This should only take a few minutes)

1. Obtain glass plates from drying rack on bench. If there is anything to clean off, use a kimwipe with DW
2. Place glass plates in green holders with the doors open, making sure both plates lay flush with the surface of the bench, and with each other. Next, while applying slight pressure to the tops of the glass plates, close the doors.
3. Place the well combs between the glass plates. Measure 11mm from the bottom of the well comb and place a mark. This is your pour line for your gel. Remove the combs and set aside.
4. Prepare 10% APS in a 1.5ml eppendorf tube: add 0.1g APS (kept at 4^{o}C) to 1ml DW. Triturate until dissolved. Make fresh daily.

5. Prepare your separating gel in a 50ml beaker with a stir bar. Your gel percentage depends on the weight of your target protein. Use the chart below to choose the appropriate percentage of gel to make.

Migration Pattern for Ready Gel Tris-HCl Gels

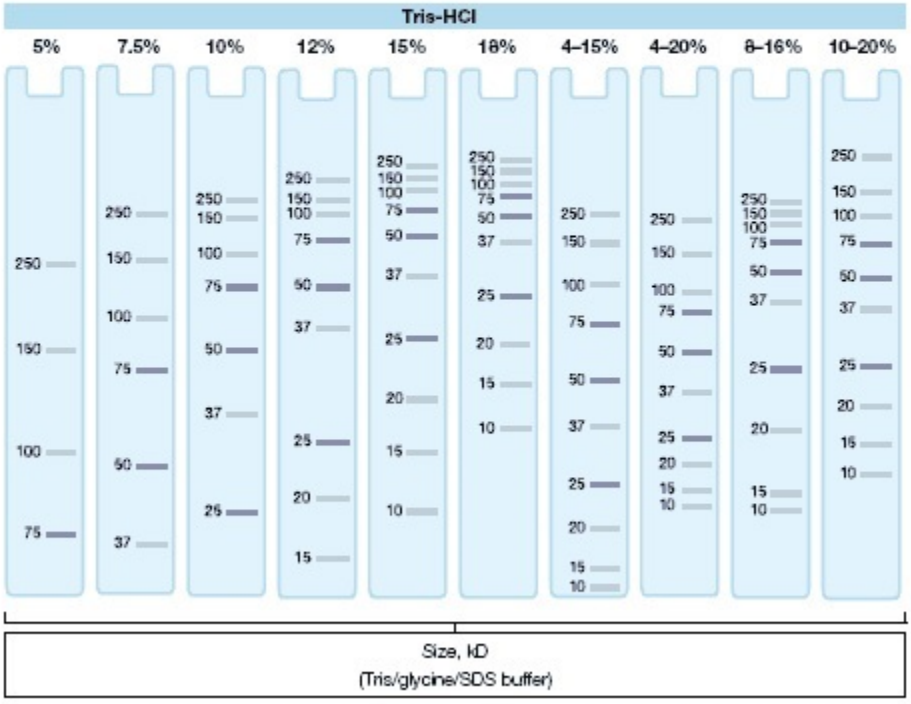

http://www.bio-rad.com/en-us/product/ready-gel-precast-gels/ready-gel-tris-hcl-precast-gels

Volume (ml)

Stock Component	5%	7.5%	10%	12%	15%
Distilled Water	12.3	10.93	9.68	8.68	7.18
1.5M Tris, pH 8.8	5	5	5	5	5
10% SDS	0.2	0.2	0.2	0.2	0.2
40% Acrylamide	2.5	3.75	5	6	7.5

The percentage of acrylamide determines the percentage of gel you are making. So, if you have 30% acrylamide to start, you will need to adjust volumes accordingly. For example, for a 10% gel, you will need 6.67ml of 30% acrylamide, and 8.01ml of DW. The DW is to make up the final volume of the solution to ~20ml.

6. Once the stock components are mixed for the appropriate separating gel percentage, place the glass plates that are in the green holders onto the sponges of the gel apparatus. Clip them in. Ensure they are sitting flush on the sponges.
7. ***See note below.** Place the beaker on a stir plate, mixing gently so as not to introduce bubbles. While mixing, quickly add 100ul 10% APS and 20ul TEMED. Allow to mix for 30 more seconds.
8. Using a transfer pipette, pipette gel mixture quickly between the plates, moving back and forth between the two sets of plates after each pipette-ful. Fill each set of plates to your marker line.
9. Carefully overlay the separating gel with 20% methanol using a syringe. Allow to polymerize for 30 mins. **Tip: leave your transfer pipette in your beaker containing left over gel solution. If this is polymerized after 30 minutes, your gel between the plates will be too.*
10. During this polymerization, mix your stock components for your stacking gel in a 50ml beaker containing a stir bar:

	Volume (ml)
Stock Component	**4%**
Distilled Water	12.68
0.5M Tris, pH 6.8	5
10% SDS	0.2
40% Acrylamide	2

Note the use of a different Tris buffer

11. Once the gel is polymerized, pour the methanol down the sink and rinse the empty area between the plates three times with 0.1% SDS in a syringe (keep gels on the apparatus during this time). Ensure all SDS is emptied from this area by tilting the apparatus to the side and holding kimwipes to the top edge of the glass plates.
12. Place the beaker on a stir plate, mixing gently. While mixing, quickly add 100ul 10% APS and 20ul TEMED. Allow to mix for 30 more seconds.
13. Using a transfer pipette, overlay the separating gel with the stacking gel solution, filling to the top of the plates. Insert comb on an angle slowly so as not to introduce bubbles or displace too much gel solution. Allow to polymerize for 30 mins

***Note**: If a vacuum degasser system is available, make up both the separating and stacking gel solutions in their beakers with stir bars (without the APS and TEMED), mix briefly on the stir plate and place both beakers into the degasser. Put the lid on and turn the vacuum pump on. Leave for 20 minutes to remove the air from the solutions. After 20 minutes, turn the pump off, remove the separating

gel, and while gently mixing on the stir plate, continue as for step 7. While the separating gel is polymerizing, put the lid back on the degasser to protect the stacking gel.

14. Put your molecular marker (ladder) on ice
15. Prepare your 1X Running Buffer as described in the Buffers section. This can be prepared in advance and stored at 4^{o}C
16. Once the gel is polymerized, remove the combs by pulling them straight up and out. Remove the glass plates carefully from the holders and place them onto the middle section of the apparatus (containing the electrodes). The short plates of each set should be facing each other. Place this section into the beige middle part with clear “doors”. The doors should be open while the electrode is being inserted. Apply gentle downward pressure to the electrode section while closing the doors. Place this in the clear container.
17. Fill the middle section between the two gels with 1X Running buffer. Next, fill the clear container half way
18. Fill a Styrofoam box with ice. Create a spot to put the gel container. Place the gel container in this spot and push the ice against the sides of the container.
19. Begin loading your samples and ladder into the wells of the gel. You should load the wells of the gel closest to you first, and then turn the whole Styrofoam box to load the other gel.
    Typically, 5ul of ladder is loaded into the first well on your left. All wells should be filled to ensure the samples run straight down.
20. Once all samples are loaded, place the lid onto the container (black to black electrode, red to red electrode). Plug the cords into the power supply and turn on. Turn the voltage up to 200V and press the button that looks like a man running. Make sure to observe bubbles in the running buffer, signifying the gel is running.
21. The samples are condensed into a solid blue line while they run through the stacking gel. This ensures that all samples enter the separating gel at the same time, and therefore have the same amount of time to run through the gel.
22. Allow your gel to run until the blue dye front completely runs off the bottom of the gel. This typically takes just over 1 hour. While this is happening, gather your transfer supplies and make fresh 1X Transfer Buffer, as per the Buffers section. This can be made in advance and stored at 4^{o}C.

Gel Transfer
What you need:
-transfer apparatus and container (bench)

-2x cassettes (bench)
-2 plastic containers for soaking filter paper, sponges, and membranes (bench)
-2 plastic containers for soaking the gels (bench)
-4x black sponges (bench)
-4x filter paper (bench)
-2x nitrocellulose membrane (bench)
-flat forceps (bench)
-1x transfer buffer (4^{o}C)
-ice pack (-20^{o}C)
-stir bar
-gel wedge

23. Once the gel is finished running, bring the entire container to the sink and dump out the running buffer. **Do not reuse this buffer.** Disassemble the apparatus to remove the glass plates.
24. Using the gel wedge, release the gel from the big plate so the gel is kept on the short plate. Cut the stacking gel off using the wedge and discard. Make a nick in the top left corner (usually the corner containing your ladder).
25. Add 1x Transfer buffer to a container. Place the short plate with the gel on it over the top of the container. By allowing the buffer to make contact with the gel, it should take the gel off of the plate itself. If this does not work, or if the gel stayed on the big plate rather than the short plate, use the wedge to gently lift the gel off of the plate and place into the buffer. Repeat with second gel in a separate plastic container.
26. Cut two membranes from the nitrocellulose roll using the filter paper as a size guide. Be careful not to touch the membrane with your gloves. Keep the blue paper on while cutting.
27. In another plastic container, place one sponge, one filter paper, one membrane, one filter paper, one sponge, and fill with 1X Transfer buffer. Repeat for second membrane.
28. Place all plastic containers on the belly dancer for 15 minutes, with slight agitation. This is necessary to equilibrate all components of the transfer “sandwich”
29. While these components are soaking, wash the running apparatus. To do this, re-assemble without the glass plates and fill the container with DW. Discard and repeat for a total of 3 times. Allow to dry on the drying rack or paper towel. **Do not hang.**
30. Assemble the sandwiches out of buffer on paper towel on the bench in the following order: clear side down, sponge, filter paper, membrane (move with forceps), gel (move with gel wedge, place so that cut corner remains on your left, ensure no bubbles), filter paper.

31. Use a 50ml tube to roll out any bubbles by starting in the middle of the filter paper and rolling outward. Repeat in opposite direction. Complete the sandwich by placing the second sponge onto the filter paper. Close the sandwich and repeat with the second one.
32. Place the sandwiches in the centre of the transfer apparatus with the black side of the cassettes facing the black side of the apparatus. Place the apparatus in the clear container (same one used for running of gel), add a stir bar, and place the ice pack in the unfilled space in the container.
33. Fill the container up to the edge with fresh 1X Transfer buffer
34. Move the apparatus to the clear door fridge onto the stir plate. Turn the stir plate on to low, making sure the stir bar moves easily. Place lid on top, red to red electrode and black to black electrode.
35. Turn the power supply on to 30V and run overnight.

Day 2 – Ponceau S, Blocking, and Primary Antibody

What you need:
-2x plastic containers (bench)
-flat forceps (bench)
-scalpel (bench)
-Ponceau S stain (bench, in the dark)
-0.1M NaOH (bench)
-1XTBST (bench)
-1 clear plastic sheet (bench)
-Blocking Solution
-primary antibody (storage conditions dependent on antibody)
-50ml conical tube

36. Press stop on the power supply, turn off the stir plate and return the apparatus to the bench.
37. On paper towel on the bench, open the sandwich (black side down) and cut the membrane to size using the scalpel, following the outline of the gel below it. If the transfer was successful, you will see the ladder on the membrane. Cut the nick in the corner again and flip the membrane over so that the nick is now on your left and place in a container. To keep track of which side is which, this nick should always be on your left, the side with your ladder. Repeat with the second sandwich.
38. Rinse the membranes with DW quickly then discard and add Ponceau S to the container (enough to cover the membrane). Place on belly dancer at low speed for 5 minutes.
39. During this staining, wash the transfer apparatus as you did the running apparatus. Allow to dry on the drying rack.

40. Discard the Ponceau stain down the sink and rinse the membranes with DW until all residual background red is gone, and only red bands remain. Scan this image on the computer.
    a. Open Canoscan
    b. Ethanol the scanner surface
    c. Lay membranes down on the surface, ensuring no bubbles
    d. Lay a clear plastic sheet over the membranes and close the scanner
    e. Select “Scan1”, source=platen, save to your file, click “ok”
    f. After the scan completes, the image is saved automatically. Check to make sure the picture is clear before destaining the membrane
    g. Ethanol the scanner surface again.
41. Destain the membranes by adding 0.1M NaOH to the container with agitation. It should destain within minutes.
42. Discard and rinse with DW, then wash the membrane for five minutes on the belly dancer at medium speed in 1XTBST (recipe in Buffers section, this can be made in advance and stored at room temperature)
43. During this wash step, prepare your blocking solution. Make sure to check the antibody information sheet of the antibody you will use to choose the appropriate blocking solution. Typically, 5% milk is sufficient, but BSA is also sometimes used. Skim milk is in a bag in the weigh room and BSA is kept at 4^{o}C. Make this fresh daily in 1XTBST. Typically, 25ml is used per membrane.
44. Once the wash step is complete, discard the 1XTBST and add blocking solution to the container. Place on the belly dancer at room temperature on a low speed for 1 hour.
    **Tip: If after you complete your western it comes out with nonspecific antibody binding, you can increase your blocking percentage to 8% to attempt to eliminate that.*
45. Just before the blocking step is complete, make up the primary antibody in a 50ml tube. The antibody information sheet should suggest a starting concentration for the antibody, as well as what to make it in. Typically, 5ml of antibody solution (5% milk or BSA made in 1XTBST) is made per membrane.
46. Once the blocking step is complete, if you are probing for multiple targets that run far enough apart on the gel, you can cut your membrane into two pieces and probe two at once. If you do this, you will cut using the scalpel, and use the smaller sectioned container. Each half of the gel should fit perfectly into the sections, allowing for the use of 2.5ml of antibody solution. If you do not cut the membrane, move the membrane to the smaller coloured containers that fit the whole membrane perfectly. This

container requires 5ml of antibody solution. Place the container of choice on the rocker in the fridge (4°C) at a low speed. Leave overnight.

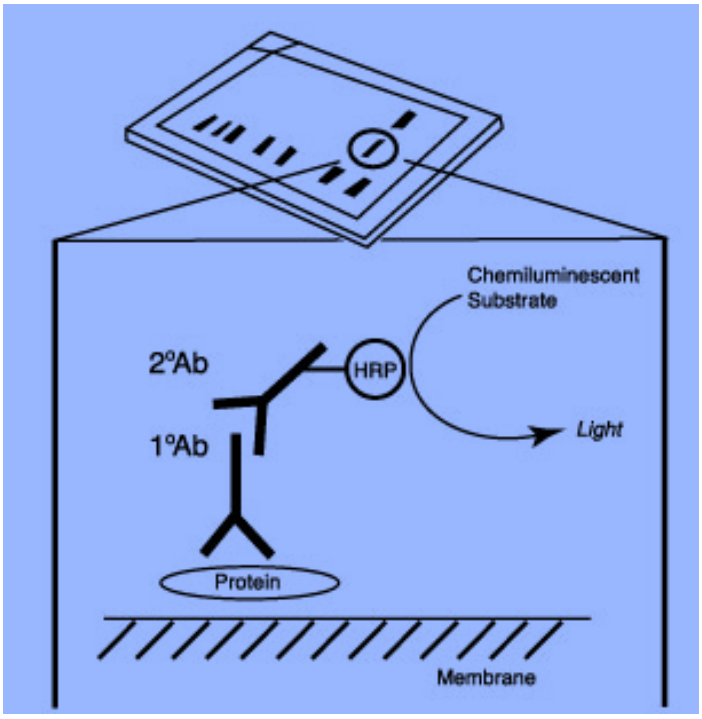

The information sheet that comes with your antibody has suggested blocking percentages as well as antibody concentrations. It also lists species reactivity, meaning which animal species they can detect. Ensure the antibody you choose is specific for the species of your sample. Some primary antibodies are specific to multiple animals. Your secondary antibody is made to target your primary antibody based on the animal that your primary antibody was made in. So, if your primary antibody is a goat anti-rat IL-6, it is detecting rat IL-6 in your sample, and was made in a goat. This means your secondary antibody must be anti-goat. Do not use a secondary antibody that is specific to your sample species. This will cause unspecific binding. So, if your sample comes from a rat, your secondary should not be anti-rat, and therefore your primary cannot be made in a rat.

Day 3 - Secondary antibody

What you need:
-2x plastic containers
-1XTBST (bench)
-Blocking solution (made fresh daily)
-secondary antibody (storage conditions dependent on antibody)
-15mL tubes (bench)

47. Remove membranes from the fridge and place in plastic containers. Add 1XTBST to cover and wash the membranes for a total time of 25 mins (medium speed on the belly dancer), changing the buffer every 5 minutes (discard down drain).
48. During the last wash, prepare the secondary antibody as per the antibody information sheet. Typically, 25ml of solution (usually in 5% milk made in 1XTBST) is used per membrane.

49. Following washes, discard the 1XTBST and add the secondary antibody solution. Place on belly dancer for 1 hour at room temperature at a low speed.
50. Discard the secondary antibody solution and perform wash steps as per step 47.
51. During the final wash steps, prepare your detection solution (If using enhanced chemiluminescence, continue as below) and set up the computer

Enhanced Chemiluminescence (ECL)

What you need:
-1XTBST (bench)
-1.0M Tris pH 8.5 (4^{o}C)
-DW
-30% H_2O_2 (4^{o}C)
-Coumeric acid - light sensitive (-20^{o}C)
-Luminol - light sensitive (-20^{o}C)
-1x clear plastic sheet (bench)
-2x 50mL tubes, one wrapped in tinfoil (bench, tinfoil in autoclave room)
-plastic wrap, taped flat to the bench
-kimwipes
-1ml pipette and tips
-flat forceps for membrane handling

*Take out coumeric acid and luminol, wrap in tinfoil and thaw on bench

Label two 50ml tubes as “Solution 1” and “Solution 2”. Add components listed below and keep solution 2 covered with tinfoil.

	Solution 1		**Solution 2**
Component	**Volume**	**Component**	**Volume**
1.0M Tris pH 8.5	2mL	1.0M Tris pH 8.5	2mL
30% H_2O_2	12uL	90mM Coumeric acid	88uL
Distilled Water	8mL	250mM Luminol	200uL
		Distilled Water	8mL

Computer Set-Up

a. Turn on the ChemiDoc imager (2 things to turn on: black box beside the computer first, then big beige imager)
b. Open “Quantity One” on the computer, press “EPI White” on the imager

c. In the program, “File” > “ChemiDox XRS” > “Select” > “Custom” > “Western MWM”
d. Change the filter on the imager to the middle position (black stick on top)

52. After the final wash, discard the wash buffer. Using the flat forceps, move the membranes to the plastic wrap.
53. Pour ECL solutions together into one 50ml tube and mix by inverting. Pipette the mixed ECL directly onto the membranes, being sure to cover every part of it. Continue for one minute.
54. Dab excess ECL solution from membranes onto kimwipe by touching the corner of the membrane to the kimwipes, handling with the flat forceps. Place membranes onto clear plastic sheet and move to imager
55. Open drawer on imager to place membranes on sheet inside. In program, click “Live Focus” > “Freeze” (once it is in the appropriate position; it can be focused using the buttons on the imager) > “Auto Expose” > “Save”. You now have an image of your ladder saved which is used to determine band size.
56. To detect your chemiluminescence, “File” > “ChemiDox XRS” > “Select” > “Custom” > “Sean Bryan Western”, turn off the “Epi White” on the imager, change the filter to the first position (a O), click “Live Acquire”, and fill in as 300 second exposure with photos taken every 60 seconds. Click “Save” and it will run. This time can be altered based on your target protein and how easily it can be imaged. You will have an idea of how well this timing is working after the first minute when the first picture pops up.
57. Once all images have been taken, the membrane can be discarded or stored at 4^{o}C in 1XTBS (1XTBST without the Tween 20) until a decision is made. The membrane can be stripped and re-probed for another target if necessary.